AD-A169 781 IODINE MONOFLUORIDE ENERGY TRANSFER STUDIES(U) ROCKWELL 1/1
INTERNATIONAL THOUSAND OAKS CA SCIENCE CENTER
A T PRITT JUN 86 SC5366.51FR AFWL-TR-85-04
UNCLASSIFIED F29601-83-C-0048 F/G 20/5 NL

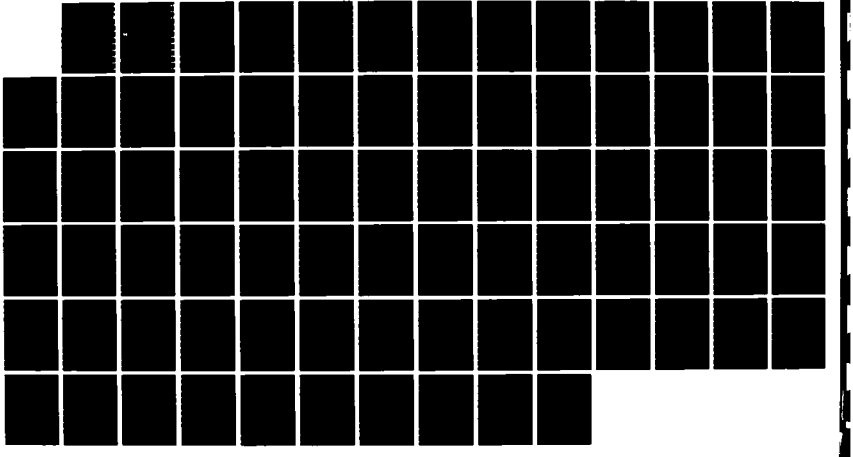

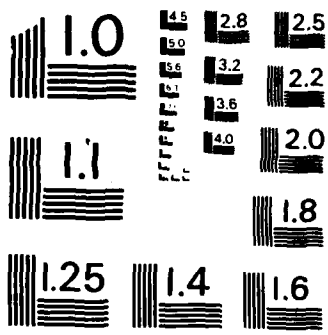

MICROCOPY RESOLUTION TEST CHART
NATIONAL BUREAU OF STANDARDS - 1963 - A

IODINE MONOFLUORIDE ENERGY TRANSFER STUDIES

A.T. Pritt

Rockwell International Science Center
1049 Camino Dos Rios
Thousand Oaks, CA 91360

June 1986

Final Report

AIR FORCE WEAPONS LABORATORY
Air Force Systems Command
Kirtland Air Force Base, NM 87117-6008

This final report was prepared by Rockwell International Science Center, Thousand Oaks, California, under Contract F29601-83-C-0048, Job Order 33260338, with the Air Force Weapons Laboratory, Kirtland Air Force Base, New Mexico. Second Lieutenant Brian McFeeters (ARDD) was the Laboratory Project Officer-in-Charge.

When Government drawings, specifications, or other data are used for any purpose other than in connection with a definitely Government-related procurement, the United States Government incurs no responsibility or any obligation whatsoever. The fact that the Government may have formulated or in any way supplied the said drawings, specifications, or other data, is not to be regarded by implication, or otherwise in any manner construed, as licensing the holder, or any other person or corporation; or as conveying any rights or permission to manufacture, use, or sell any patented invention that may in any way be related thereto.

This report has been authored by a contractor of the United States Government. Accordingly, the United States Government retains a nonexclusive, royalty-free license to publish or reproduce the material contained herein, or allow others to do so, for the United States Government purposes.

This report has been reviewed by the Public Affairs Office and is releasable to the National Technical Information Services (NTIS). At NTIS, it will be available to the general public, including foreign nations.

If your address has changed, if you wish to be removed from our mailing list, or if your organization no longer employs the addressee, please notify AFWL/ARDD, Kirtland AFB, NM 87117-6008 to help us maintain a current mailing list.

This technical report has been reviewed and is approved for publication.

BRIAN MC FEETERS
2Lt, USAF
Project Officer

FOR THE COMMANDER

ORVEN F. SWENSON
Major, USAF
Chief, Short Wavelength Laser Branch

HARRO ACKERMANN
Lt Col, USAF
Chief, Laser Science & Tech Office

DO NOT RETURN COPIES OF THIS REPORT UNLESS CONTRACTUAL OBLIGATIONS OR NOTICE ON A SPECIFIC DOCUMENT REQUIRES THAT IT BE RETURNED.

UNCLASSIFIED
SECURITY CLASSIFICATION OF THIS PAGE

REPORT DOCUMENTATION PAGE

1a. REPORT SECURITY CLASSIFICATION Unclassified	1b. RESTRICTIVE MARKINGS
2a. SECURITY CLASSIFICATION AUTHORITY	3. DISTRIBUTION/AVAILABILITY OF REPORT Approved for public release; distribution unlimited.
2b. DECLASSIFICATION/DOWNGRADING SCHEDULE	
4. PERFORMING ORGANIZATION REPORT NUMBER(S) SC5366.51FR	5. MONITORING ORGANIZATION REPORT NUMBER(S) AFWL-TR-85-04
6a. NAME OF PERFORMING ORGANIZATION Rockwell International Science Center 6b. OFFICE SYMBOL (If applicable)	7a. NAME OF MONITORING ORGANIZATION Air Force Weapons Laboratory
6c. ADDRESS (City, State, and ZIP Code) 1049 Camino Dos Rios Thousand Oaks CA 91360	7b. ADDRESS (City, State, and ZIP Code) Kirtland Air Force Base NM 87117-6008
8a. NAME OF FUNDING/SPONSORING ORGANIZATION 8b. OFFICE SYMBOL (If applicable)	9. PROCUREMENT INSTRUMENT IDENTIFICATION NUMBER F29601-83-C-0048
8c. ADDRESS (City, State, and ZIP Code)	10. SOURCE OF FUNDING NUMBERS PROGRAM ELEMENT NO: 62601F; PROJECT NO: 3326; TASK NO: 03; WORK UNIT ACCESSION NO: 38

11. TITLE (Include Security Classification)
IODINE MONOFLUORIDE ENERGY TRANSFER STUDIES

12. PERSONAL AUTHOR(S)
Pritt, A. T.

13a. TYPE OF REPORT	13b. TIME COVERED	14. DATE OF REPORT (Year, Month, Day)	15. PAGE COUNT
Final	FROM 83-06-13 TO 84-10-31	1986, June	78

16. SUPPLEMENTARY NOTATION

17. COSATI CODES		
FIELD	GROUP	SUB-GROUP
20	05	
10	01	

18. SUBJECT TERMS (Continue on reverse if necessary and identify by block number)
Chemical Laser; Electronic Energy Transfer; Chemiluminescence; Energy Transfer Efficiency; Iodine Monofluoride; Nitrogen Monofluoride; (over)

19. ABSTRACT (Continue on reverse if necessary and identify by block number)
Electronic-to-electronic (E-E) energy transfer from $NF(b^1\Sigma^+)$ to $IF(X^1\Sigma^+)$, producing $IF(B^3\Pi(0^+))$, was investigated using both spatially resolved data from a chemiluminescence flow tube apparatus and temporarily resolved data following pulsed excitation in a flow tube. The $b^1\Sigma^+$ state of NF was generated by the $F+HN_3$ reaction under steady-state flow tube conditions and by the $NF(a^1\Delta)+I^*$ pooling reaction for the temporally resolved studies. Results of this study show that the source of $IF(B^3\Pi(0^+))$ in these chemiluminescence reactions stems from E-E energy transfer, that the rate of the transfer reaction depends strongly on the vibrational distribution in the ground state of IF, that the rate is independent of the vibrational distribution in the $NF(b^1\Sigma^+)$, and that the efficiency of the transfer rate is greater than 20%. The rate constant for the E-E energy transfer was measured to be $1.5 \pm 0.2 \times 10^{-11}$ cm^3/molecule^{-1} s^{-1} for an $IF(X^1\Sigma^+)$ vibrational distribution corresponding to 800 K. These results are explained in terms of an energy transfer mechanism requiring that the individual state-to-state rates are proportional to the probabilities associated with vertical transitions.

20. DISTRIBUTION/AVAILABILITY OF ABSTRACT ☒ UNCLASSIFIED/UNLIMITED ☐ SAME AS RPT ☐ DTIC USERS	21. ABSTRACT SECURITY CLASSIFICATION Unclassified
22a. NAME OF RESPONSIBLE INDIVIDUAL 2Lt Brian McFeeters	22b. TELEPHONE (Include Area Code) (505) 844-1871 22c. OFFICE SYMBOL AFWL-ARDD

DD FORM 1473, 84 MAR 83 APR edition may be used until exhausted. All other editions are obsolete

SECURITY CLASSIFICATION OF THIS PAGE
UNCLASSIFIED

18. SUBJECT TERMS (Continued)

Pumping Mechanism.

CONTENTS

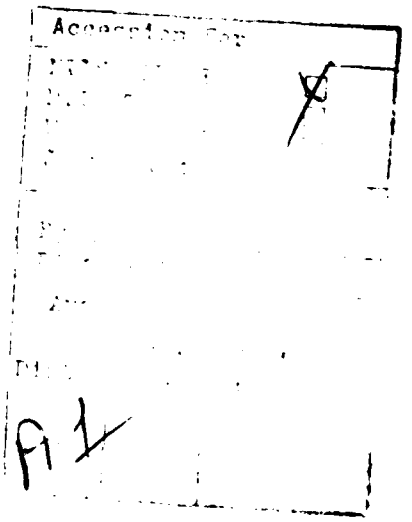

ILLUSTRATIONS

ILLUSTRATIONS (Continued)

ILLUSTRATIONS (Continued)

TABLES

I. INTRODUCTION

Short wavelength chemically driven lasers have been identified as having potential for high-energy thermal weapons in both atmospheric and space environments. To date, however, no purely chemically driven reaction system has shown promise for developing a short-wavelength laser. The only continuous wave (CW) electronic transition laser operating on a purely chemical basis is the oxygen-iodine energy transfer laser at 1.3 μm. The success of this laser has spurred increased activity in studying electronic-to-electronic (E-E) energy transfer processes as a means of extracting energy from chemically generated, radiatively metastable species. In recent years, $NF(a^1\Delta)$ and $NF(b^1\Sigma^+)^*$ have been chemically generated in large flows commensurate with the above mission requirements (Refs. 1 and 2).

A number of lasers operating at visible wavelengths have been developed by direct optical pumping. Diatomic species such as the halogen and interhalogen species have been shown to lase both by pulsed and CW optical pumping (Refs. 3-7). The success of these halogen systems lies in the displaced energy potentials between the ground state and the optically pumped state. Recently, iodine monofluoride (IF) was optically pumped using a pulsed dye laser to obtain lasing at low pressures (Ref. 8) while lasing from the lowest vibrational levels was demonstrated (Ref. 9) at higher pressures. Finding a collisional analog to the optical pumping approach using known chemically generated metastable species would therefore be interesting.

---

*Hereafter NF(b) and NF(a) refer to $NF(b^1\Sigma^+)$ and $NF(a^1\Delta)$, respectively.

Ref. 1 J.M. Herbelin, D.J. Spencer, and M.A. Kwok, J. Appl. Phys. 48, 3050 (1977).

Ref. 2 J.M. Herbelin, M.A. Kwok, and D.J. Spencer, J. Appl. Phys. 49, 3750 (1978).

Ref. 3 P.L. Byer, R.L. Herbst, H. Kildal, and M.D. Levenson, Appl. Phys Lett. 20, 463 (1972).

The production of $IF(B^3\Pi(0^+))^*$ was observed when either CF_3I or I_2 was added to a reacting mixture of F + HN_3 (Ref. 10). Furthermore, the B state of IF appeared only in the presence of NF(b). The electronic energy of NF(b) is nearly resonant to the energy difference between the ground state and B state of IF, suggesting that a near-resonant E-E energy transfer process from NF(b) to $IF(X^1\Sigma^+)$ is responsible for the observed production of the IF B-X emissions. The present study continued the earlier reported observations by verifying that the production of IF(B) is via E-E energy transfer from NF(b), by measuring the E-E energy transfer rate constant as a function of the vibrational distribution in NF(b) and in IF(X), and by determining a lower bound for the efficiency of the transfer process.

The following section describes the experimental apparatus consisting of a chemiluminescence flow tube, associated gas handling system, and the diagnostics used in the program. A review of novel means of generating NF(b) by both CW and pulsed methods is given in Section III. Section IV presents the results and analyses used to verify the E-E energy transfer process involving NF(b) and to determine the E-E energy transfer rate constant. The data were collected as a function of reagent stoichiometries, of the vibrational distibution in the NF(b) state, of the vibrational distribution in the IF ground state, and of the position along the chemiluminescence flow tube. The results used to determine the efficiency of the E-E energy transfer process are presented in Section V. Both CW and pulsed methods were used to determine the efficiency. Section VI presents a discussion of the mechanisms for E-E energy transfer processes, in general, and for energy transfer in NF/IF, in particular. A discussion of our present understanding of the NF/IF E-E energy transfer system and of the requirements for developing a chemical

*Hereafter, IF(B) and IF(X) refer to $IF(B^3\Pi(0^+))$ and $IF(X^1\Sigma^+)$, respectively.

Ref. 4 S.R. Leone and K.G. Kosnik, Appl. Phys. Lett. 30, 346 (1977).
Ref. 5 F.J. Wodarczyk and H.R. Schlossberg, J. Chem. Phys. 67, 4476 (1977).
Ref. 6 W.P. West and H.P. Broida, Chem. Phys. Lett. 56, 283 (1978).

laser is also presented. A listing of critical factors associated with this laser concept is supplied, and a plan on how best to proceed with its realization with minimum risk is suggested. Finally new chemical systems which include metastable generators and associated energy transfer schemes are suggested for future study.

Ref. 7 J.B. Koffend and R.W. Field, J. Appl. Phys. 67, 4476 (1977).
Ref. 8 S.J. Davis and L. Hanko, Appl. Phys. Lett. 37, 692 (1980).
Ref. 9 S.J. Davis, L. Hanko, and R.F. Shea, J. Chem. Phys. 78, 172 (1983).

II. EXPERIMENTAL DETAILS

All experiments for this study were conducted in a chemiluminescence flow tube. Each specific experiment required some modification to the flow tube to accommodate either the arrangement of the flows in the flow tube or the position of various diagnostic equipment. An overall schematic of the flow tube with some of the basic diagnostics is presented in Figure 1.

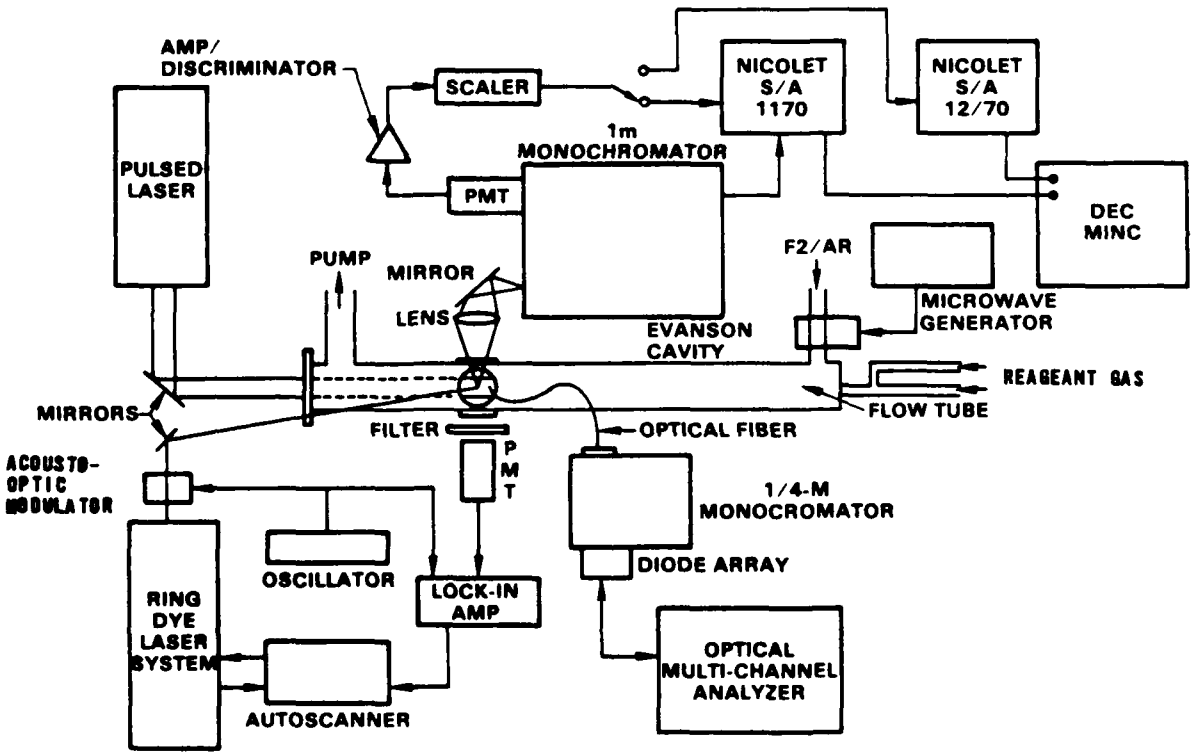

Fig. 1 Schematic of chemiluminescence flow tube apparatus, showing some of the major diagnostics.

1. THE CHEMILUMINESCENCE FLOW TUBE

The flow tube was constructed out of 1.25-in.*-diameter (inside) stainless steel whose internal surfaces were coated with Teflon. A 0.5-in. tube was welded to the upstream side. A 0.5-in. alumina tube was attached to this port via Ultra Torr fittings for introduction of the fluorine gas mixture. An Evanson cavity was used to couple energy from a 1.24-GHz 100-W microwave power supply (Raytheon). On the downstream side of the flow tube were positioned four 1.0-in.-diameter sapphire windows equally around the waist of the flow tube, each viewing the same point along the flow. At the most downstream point of the flow tube was a 1.0-in.-diameter port for the gases to exit the flow tube. A 2.0-in.-diameter CaF_2 window terminated the downstream side of the flow tube. The gases in the flow tube were evacuated either by a 500 CFM** pump (Kinney) or by a 300 CFM Stokes roughing pump and a 3000 CFM Roots blower positioned between the pump and the flow tube.

A dual-staged injector system of concentric design was inserted into the upstream side of the flow tube. A schematic of this injector tube assembly is shown in Figure 2. Reagent gases could be passed through either the central injector or through the annular injector, depending on the order by which the reagents were to be added to the flow. The distance between the annular injector and the central injector could be varied between 1-8 cm. The annular injector consisted of 32 holes (0.020-in. diameter), positioned equally around the injector tube assembly, thus spraying the reagent gases at right angles to the direction of flow in the outer annulus of the flow tube. The central injector consisted of 16 holes (0.024-in. diameter), also equally positioned around the central tube for spraying its contents at right angles to the bulk flow in the flow tube. Both of the injector pieces were spray

---

Ref. 10 A.T. Pritt, Jr., D. Patel, and D.J. Benard, Chem. Phys. Lett. 97, 471 (1983).

* To convert inches to meters, multiply by 2.540000*E-02.
** To convert CFM to m^3s, multiply by 4.72*E-03.

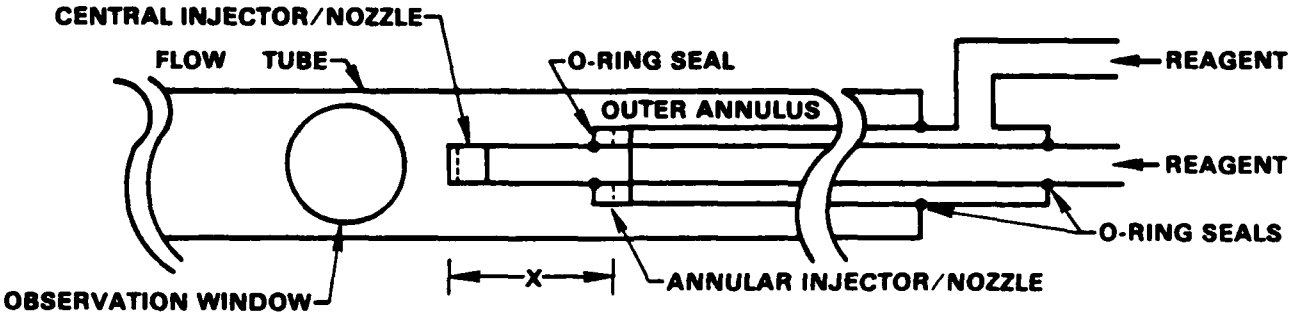

Fig. 2 Schematic of the concentric dual injection tube assembly.

nozzles which could be individually mated to the rest of the injector tube assembly. Hence, the spray nozzle assembly could be removed, and nozzles of different design could be easily installed. Once the concentric injector tube assembly was installed into the flow tube, the entire assembly could be moved with respect to the stationary observation ports. By moving the injector tube assembly and by monitoring the emissions at the observation port, one could obtain spatially resolved chemiluminescence. The outer pieces of the injector tube assembly were also coated with Teflon to minimize halogen atom recombination.

The degree of mixing of the reagents was investigated by observing the radial distribution of chemiluminescence generated in the flow tube. Photographs of the F + HN_3 flame were taken through the large diameter window at the extreme downstream end of the flow tube. In the F + HN_3 flame, the only spectral feature which exposed the film was the NF b-X emission at

529 nm. When CF_3I was added to the flame, the characteristic green flame was converted to a more intense yellow flame, corresponding to the IF B-X banded emissions. Under these conditions, the integrated intensity of the flame was about six times that of the NF b-X emission intensity. This increased intensity was noted because the film required less time for comparable exposures. The photographs were developed and the optical density was recorded by measuring the attenuation of a HeNe laser beam which was passed through the film. The HeNe laser beam, after passage through the film, was monitored by a PIN photodiode biased to 15 volts. The photocurrent was then monitored as the film was moved on an X-Y translation stage, having a resolution of 0.002 in. The results of the scans are displayed in Figure 3. For the NF b-X emissions, the distribution is relatively flat over 90% of the diameter of the flow tube, dropping precipitously at the edges of the flow tube, presumably due to wall quenching effects. The IF B-X emissions, on the other hand, show a clearly defined dip in the center of the flow tube. This dip is the shadow of the central injector through which the CF_3I was added to the flow. This shadow indicates the lack of mixing over the time frame of the flame distance. The flame becomes longer when the reagent concentrations (primarily the F_2 concentration) is reduced. The shadow effect begins to disappear under these conditions. The shadow, as seen in Figure 3b, is also easily observed when viewing the flame from the end of the flow tube.

2. GAS HANDLING SYSTEM

Each of the reagent gases were individually monitored for their flow rates using mass flow meters (Tylan). In addition, each reagent gas was paired by a separate argon gas flow. The purpose of the second argon flow was to vary the fraction of the reagent in the combined flows without changing the sum flow of both the reagent and buffer gas. Figure 4 shows a schematic diagram of the gas handling system. Each flow meter was calibrated to known N_2 flows. Individual flow rates were determined by multiplication of a correction factor supplied by the manufacturer. Each of the flows was

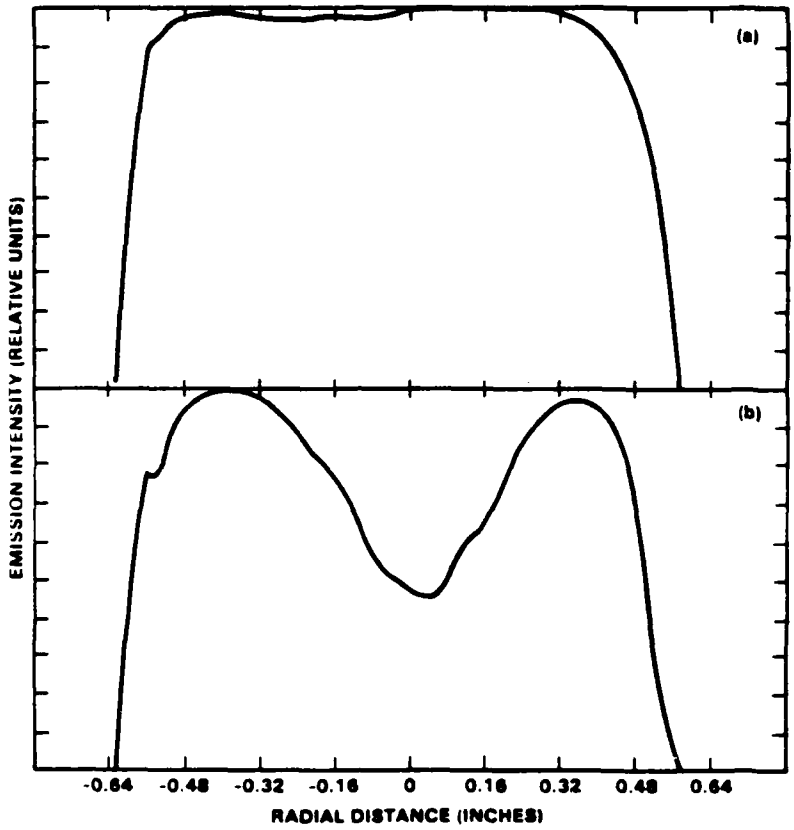

Fig. 3 Radial distribution of emissions in the chemiluminescence flow tube. [(a) Radial distribution of the NF b-X emission resulting from the addition of ~ 3 mtorr of HN_3 and 35 mtorr of F atoms (assuming 50% dissociation of F_2) at a total pressure of 800 mtorr. (b) Radial distribution of the IF B-X emission when ~ 3 mtorr of CF_3I was added to the flow resulting in a total pressure of 830 mtorr.]*

directed through 1/4-in. stainless steel tubing and regulated by a stainless metering valve. The flows of HN_3 or of the iodine bearing compound were passed through a combination of three-wave valves, so that either or both of the reagents (HN_3 or RI) could be introduced into either injector (the annular injector or the central injector, see Fig. 2) in the injector tube assembly.

---

* To convert torr to pascal (Pa) multiply by 1.333 22 E+02.

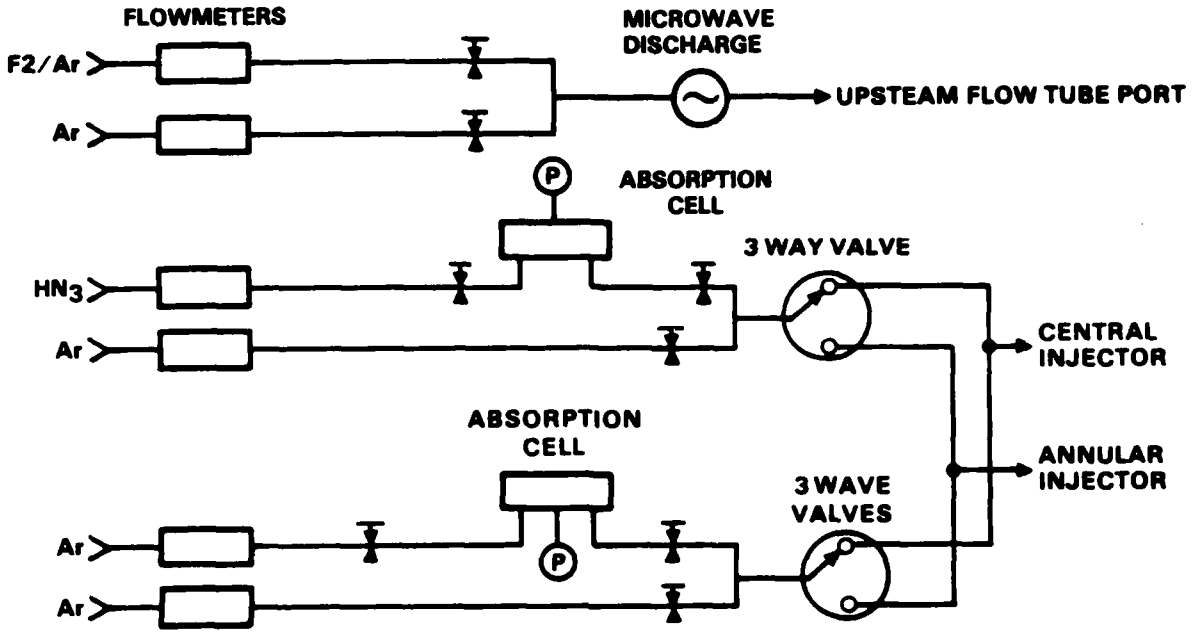

Fig. 4 Gas flow handling system.

Hydrogen azide (HN_3) was generated in a manner described previously (Ref. 11). Briefly, a 75% (by vol.) solution of H_2SO_4 or D_2SO_4 was added dropwise by a syringe pump to a bed of NaN_3 crystals, while argon gas was passed through the glass generator at room pressure. A schematic of the generator is presented in Figure 5. The wet gas leaving the generator was passed through a drying column containing $CaSO_4$ (Drierite). The entire generator sat in a fume hood. A small portion of the total gas flow was extracted past the drying column and directed through a mass flow meter and

---

Ref. 11 R.D. Coombe, D. Patel, A.T. Pritt, Jr., and J.J. Wodarazyk, Chemical Production of Excited NF, AFWL-TR-81-211, Air Force Weapons Laboratory, Kirtland AFB, NM, July 1982.

into a UV absorption spectrometer (Pie Unicam, Model 6-550). The wavelength setting of the absorption cell was set to 210 nm, a point at which the HN_3 absorption coefficient is relatively insensitive to wavelength and is well known (Ref. 12). The pressure in the absorption cell was continuously monitored by a Validyne inductance transducer.

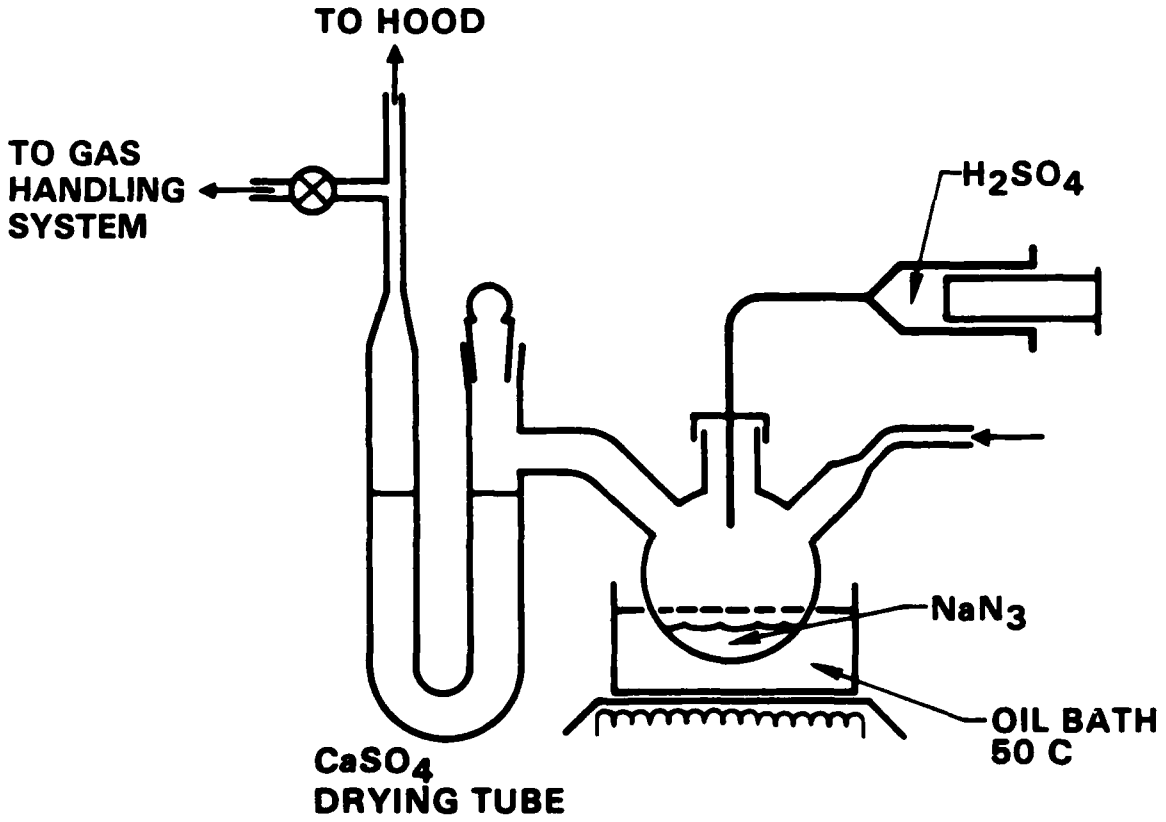

Fig. 5 Small-scale apparatus for the generation of gas phase HN_3.

When CF_3I was used as the source of IF in the flow tube, argon at reduced pressure bubbled through CF_3I liquid held at 196 K (dry ice temper-

Ref. 12 J.R. McDonald, J.W. Rabalais, and S.P. McGlynn, J. Chem. Phys. 52, 1332 (1970).

ature). The gas was then sent through a 4.7-cm-long UV absorption cell. A D_2 lamp served as the radiation source, and a 1/8-m monochromator fitted with a 2400 lines/mm grating, served as a wavelength dispersing element. The lamp intensity was detected by a 1P28 photomultiplier tube whose photocurrent was monitored by a Keithley electrometer (Model 610B). The absorption measurement was made at 250 nm, for which the absorption coefficient is known (Ref. 8). The peak of the absorption occurs at 270 nm, but in practice it was found that at this wavelength the absorption in the cell was too strong to render an accurate determination of the CF_3I pressure. The total pressure in the absorption cell was monitored by another Validyne inductance transducer. The above experimental apparatus was also used for determining the flow rate of DI.

For the experiments requiring I_2 as a source of iodine atoms and of IF, a much longer absorption cell was required since the vapor pressure of I_2 at room temperature is low (200 mtorr) (Ref. 13) and the absorption coefficient, weak (Ref. 14). Argon gas was passed over a bed of iodine crystals and into the 120-cm-long × 1-in.-diameter absorption cell. A microscope illuminator fitted with a long passband filter (> 450 nm) was used as the radiation source. A second 1P28 photomultiplier tube was used to monitor the transmitted intensity. A Corion narrow-band interference filter, centered at 490 nm with a band width of 50 nm, was placed between the absorption cell and the PMT. The photocurrent was also recorded by the Keithley electrometer (Model 610B). The total pressure in the absorption cell was monitored by a Baratron capacitance manometer.

The molecular fluorine used in this study was a mixture of 5-7.5% F_2 diluted in argon supplied by Matheson or Air Products. The purity of the gas was set by the purity of the fluorine added to the tank. The F_2 had a typical

---

Ref. 13 L. Gillespie and L. Fraser, J. Amer. Chem. Soc. 58, 2260 (1936).
Ref. 14 J.G. Calvert and J.N. Pitts, Photochemistry (John Wiley and Sons, Inc., New York, 1966) 184.

purity rating of 98%, with the balance mainly air. Purifying the O_2 and N_2 from fluorine is difficult since the freezing point for these gases are similar. This small impurity is not expected to cause any interference in the experiments in this study. The argon gas used for the buffered flows (Air Products) had a stated purity of 99.999%. Trifluoromethyliodide (CF_3I) supplied by PCR, Inc., when used as the source for IF in the flow tube apparatus, was purified by freeze-(77-K) pump-thaw cycles. When CF_3I was used as the source for the I* laser, purification was generally not necessary as long as the energy produced for each laser firing exceeded 50 mJ. Iodoheptafluoropropane (C_3F_7I) also supplied by PCR, Inc., was purified by freeze-pump-thaw cycles. Lengthy exposure to room lights resulted in a pinkish tinge which was due to decomposition. The color, however, was readily removed by adding either Cu or Zn fillings to the liquid. Sublimed iodine crystals were provided by J.T. Baker and were not further purified prior to use.

3. DIAGNOSTICS

The main diagnostic used in these experiments was a 1-m spectrometer, consisting of a 1-m Czerny-Turner design ITT monochromator with a 6-in.-square grating with 1200 line/mm ruling blazed at 500 nm. Attached to the exit slit of the monochromator was a GaAs end-on photomultiplier tube (PMT, RCA C31034) cooled to -20°C by a Products for Research thermoelectric housing. The housing also contained magnetic shielding for the PMT. The photoelectric pulses were passed through an SSR Model 1200 amplifier-discriminator system and the pulses counted by an SSR Model 1108 scaler. The pulses were converted from ECL to TTL logic and sent to the input port of either a Nicolet 11/70 or 12/70 signal averager. Emissions from the flow tube were collected by a 2-in.-diameter lens (focal length of 6 in.). The lens was positioned 12 in. from the source and 12 in. from the entrance slit of the monochromator; thus the imaging ratio was 1:1. Since the focusing lens was made of Pyrex, emissions in the UV region (< 300 nm) were not transmitted.

Spectra were recorded by the Nicolet 11/70 signal averager by counting the photon pulses in the mutichannel analyzer (MCS) mode. The channel bins were stepped synchronously with the scan of the monochromator. After scanning 0.1 nm, the monochromator issued a 5-V pulse, which was used to trigger the advance of the channel bins. The slits on the monochromator were set to 250 μm, which corresponds to a resolution of 0.2 nm; hence, the scan rate did not limit the instrument resolution. Recorded spectra were sent in digital form to a DEC MINC computer via an RS-232C serial port for storage and subsequent analysis.

The spectrometer system was calibrated for relative spectral transmission using the O + NO flame for which the absolute spectral distribution is known (Ref. 15). To obtain the O + NO spectra, nitrogen gas was passed through the microwave generator, where the F_2/Ar gas mixture normally is passed. A 3.0% NO in argon mixture was then added downstream through one of the injector ports. As long as the NO concentration was in excess of the N atom concentration, the O + NO flame could be observed. A spectrum of the F + HN_3 + I_2 flame in the 450-600 nm region is shown in Figure 6. In addition to the spectrum, the spectral response of the spectrometer system is shown by the broken line. For the pulsed laser studies, the output from the PMT which was attached to the 1-m monochromator was sent to the Nicolet 12/70 signal averager for temporally resolved data. The signal averager was operated in its MCS mode, but the channel bins were advanced by an internal clock. For these experiments, the sweep rate was at its maximum value of 500 kHz (i.e., 2 μs per bin), and the slits of the spectrometer were opened to 2 mm, representing a resolution of 1.6 nm. The digitally stored data in the Nicolet 12/70 were also sent to the laboratory computer.

Ref. 15 A. Fontijn, C.B. Meyer, and H.I. Schiff, J. Chem. Phys. 40, 64 (1964).

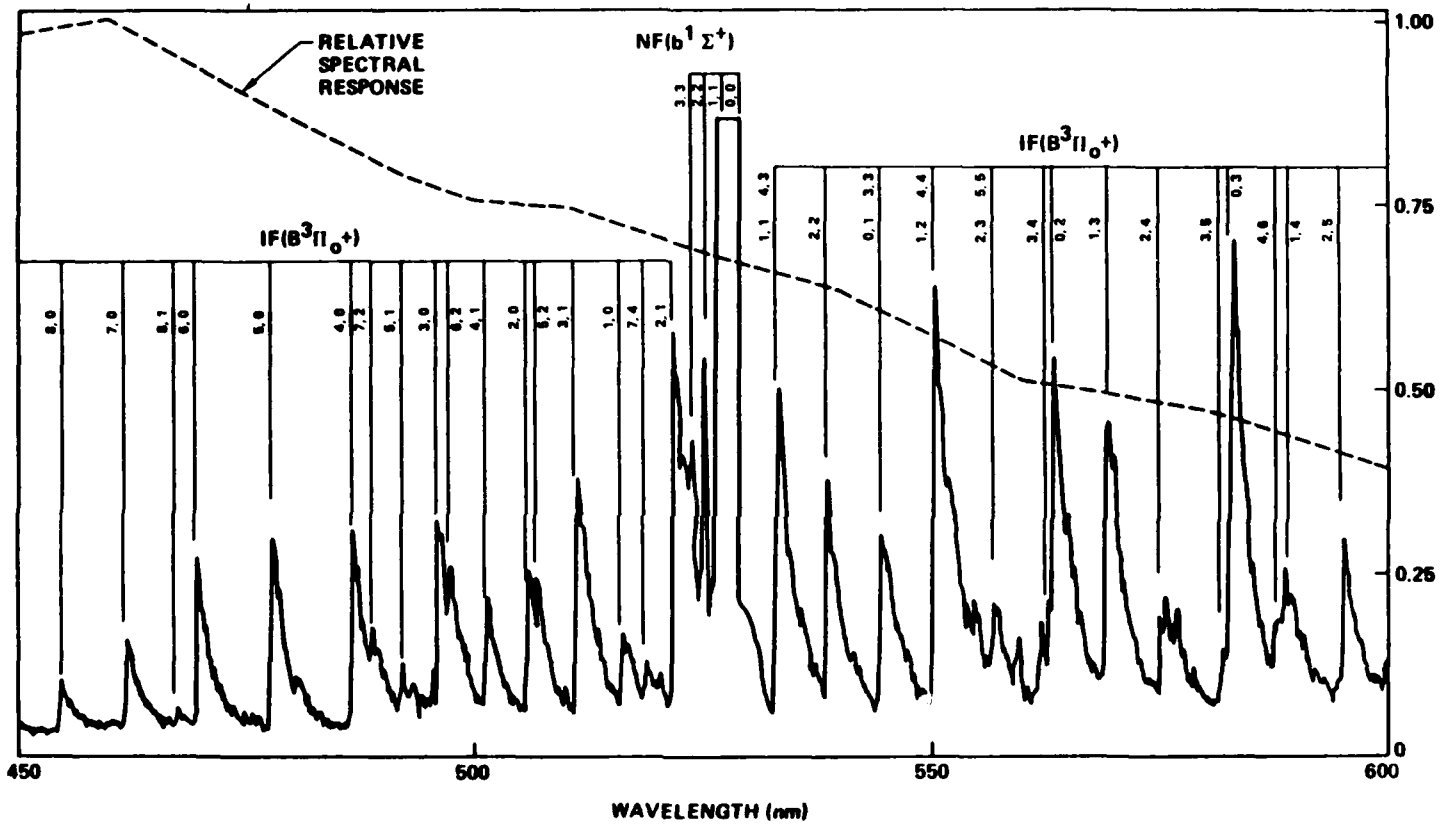

Fig. 6 Typical spectrum of the F + HN_3 + $CF_3I(I_2)$ flame. (The dashed line refers to the sensitivity response of the visible spectrometer, including focusing optics, monochromator, and photomultiplier tube.)

For the pulsed experiments, an optical multichannel analyzer (OMA) was used to obtain spectra for short time periods. A 1024-element diode array was attached to the exit plane of a 1/4-m Jarrel-Ash monochromator fitted with a 600 line/mm holographic grating. The signal diode array was driven by a Tracor Northern Analyzer Model 1710-21A. The diode array was switched into operation by a high voltage pulse during a selected time period. Since the sweep mechanism of the diode array even under pulsed operations was fixed, the trigger to the laser, which was used to generate the emissions, had to be emitted relative to the fixed sweep of the optical analyzer. A schematic of the electronics used to slave the laser trigger to the OMA is shown in Figure 7.

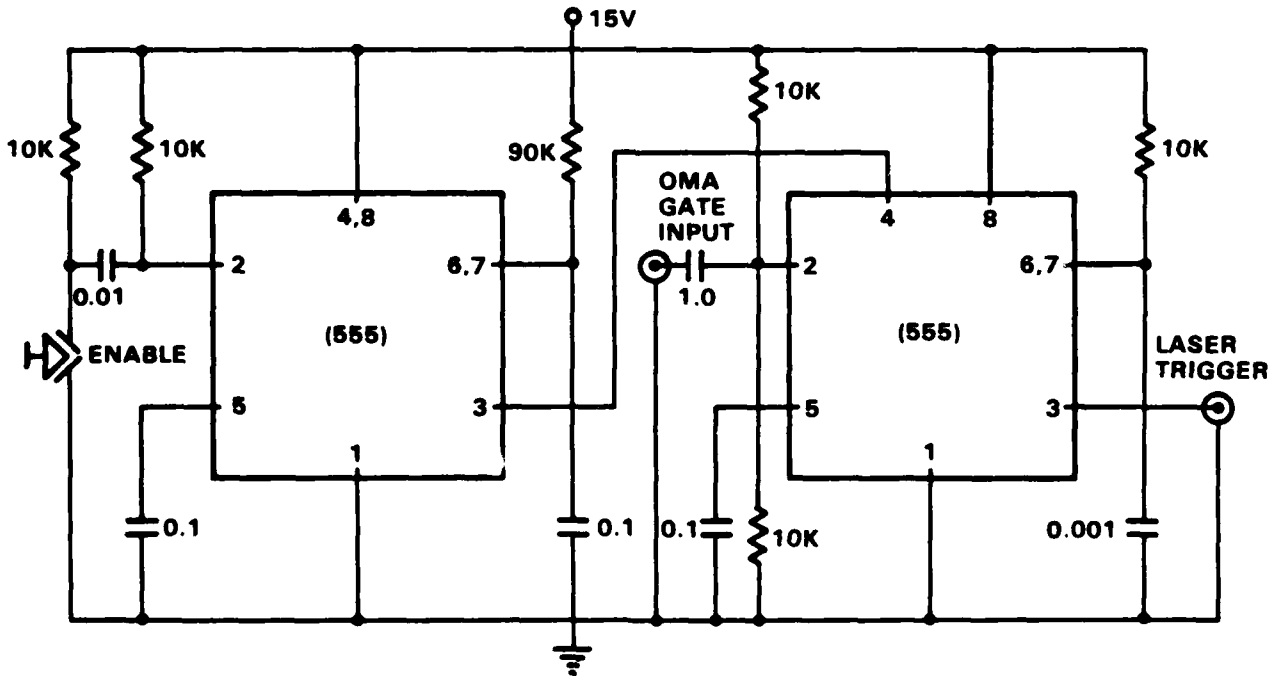

Fig. 7 Timing circuit to slave laser trigger to diode sweep of the OMA.

Laser-induced fluorescence (LIF) of IF was used to monitor its concentration in the ground state and to measure its vibrational and rotational temperature. A Coherent 699-29 ring-dye laser system fitted with an Autoscanner™ was used as the LIF diagnostic. An argon ion laser was used as the pump source for the ring-dye laser; Rhodamine 110 was used as the dye. Only the v"=1 and v"=2 levels of IF(X) could be probed with this dye. The output of the ring-dye laser was sent through an acousto-optic modulation (which was driven by an oscillator at 6 kHz) through a collimating telescope, and through the flow tube observation ports from top to bottom. At right angles to the laser path, another GaAs PMT was positioned and fitted with a long-pass filter, which transmitted wavelengths greater than 600 nm. This cutoff filter prevented the laser light from reaching the PMT, but did pass some of the fluorescence on the B-X transition of IF produced by laser excitation. The photoelectric current from the PMT was sent to a lock-in amplifier which was gated by the same oscillator which drove the acousto-optic crystal. At 6 kHz, the LIF signal was in-phase with the laser oscillation since the lifetime of the IF emission is on the order of 7-8 μs. The output of the lock-in amplifier was sent to one of the signal inputs of the Autoscanner, which digitized the signal as its scanned the laser frequency under computer control. LIF spectra were thus obtained and an example is shown in Figure 8. The positions of the ro-vibrational lines shown in Figure 8 can be compared to those which can be calculated using the spectroscopic constants for the B-X transition in IF, as reported by Trickl and Wanner (Ref. 16). Table 1 presents the observed lines and those calculated, showing agreement of the predicted and observed values. Unfortunately, the line widths obtained in this spectrum do not show any of the spectral asymmetry one might expect due to the underlying hyperfine structure. The temperature in the flow tube for which these spectra were taken was approximately 550 K, for which the Doppler line width is 730 MHz.

Ref. 16 T. Trickl and J. Wanner, J. Mol. Spectrosc. 104, 174 (1984).

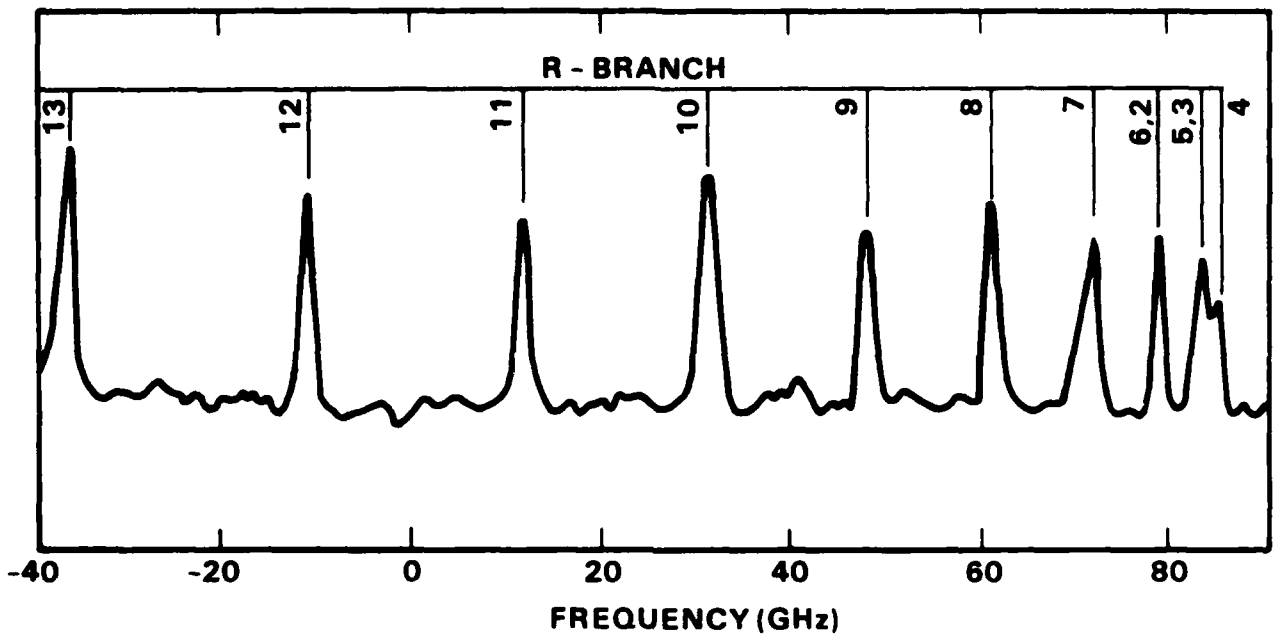

Fig. 8 High resolution excitation spectrum of the 0-1 band of the IF B-X transition at the band head. (Zero frequency is 18347.3512 cm^{-1} (545.938 nm). The P branch is unresolved from the stronger R branch in this spectral region. Resolution was limited by the Doppler linewidth associated with the transition. Molecular IF was generated by the F + I_2 reaction.)

Since IF(X) is chemically unstable, the LIF diagnostic was used to monitor its relative concentration along the flow tube. The output of the ring-dye laser was tuned to one of the ro-vibrational lines in the IF B-X bands and passed through the observation port of the flow tube. The LIF signal was monitored for the same ro-vibrational line (typically R(30)) for both the 1-1 and the 1-2 bands of the IF B-X transition as the injector tube assembly was moved with respect to the observation port. The ground state vibrational temperature for each point in the flow was determined by comparing the LIF signal for the two bands, which were pumped by the dye laser. Since the same upper state is reached in both transitions, the LIF signal strength

TABLE 1

COMPARISON OF THE MEASURED AND CALCULATED (REF.1) SPECTRAL LINES IN THE 0,1 BAND OF THE IF B-X TRANSITION

Assignment	Frequency of the Transition (cm^{-1})	
	Measured	Calculated
P(18)	18323.606	18323.598
R(27)	18323.663	18323.664
P(16)	18328.002	18328.014
R(25)	18328.099	18328.080
R(20)	18337.345	18337.357
R(13)	18346.143	18346.127
R(12)	18346.982	18346.975
R(11)	18347.730	18347.725
R(10)	18349.378	18348.373
R(8)	18349.375	18349.375

is directly proportional to the concentration of the v" levels (v"=1 and v"=2) in the ground state after correcting for their respective Franck-Condon factors (Ref. 17) and the laser power. For these experiments, the laser power was below the saturation level, as evidenced by the linearity of the LIF signal as the laser power was varied. Figure 9a shows a plot of the vibrational temperature of IF(X) vs distance down the flow tube. If we assume that the vibrational temperature is the thermal temperature, we can determine the relative concentration of IF along the flow tube. A plot of the relative concentration is shown in Figure 9b. As can be observed in the plot, the IF density drops rapidly at first and then decays at a slower rate thereafter.

Ref. 17 M.A.A. Clyne and I.S. McDermid, J. Chem. Soc. (Faraday II) 72, 252 (1976).

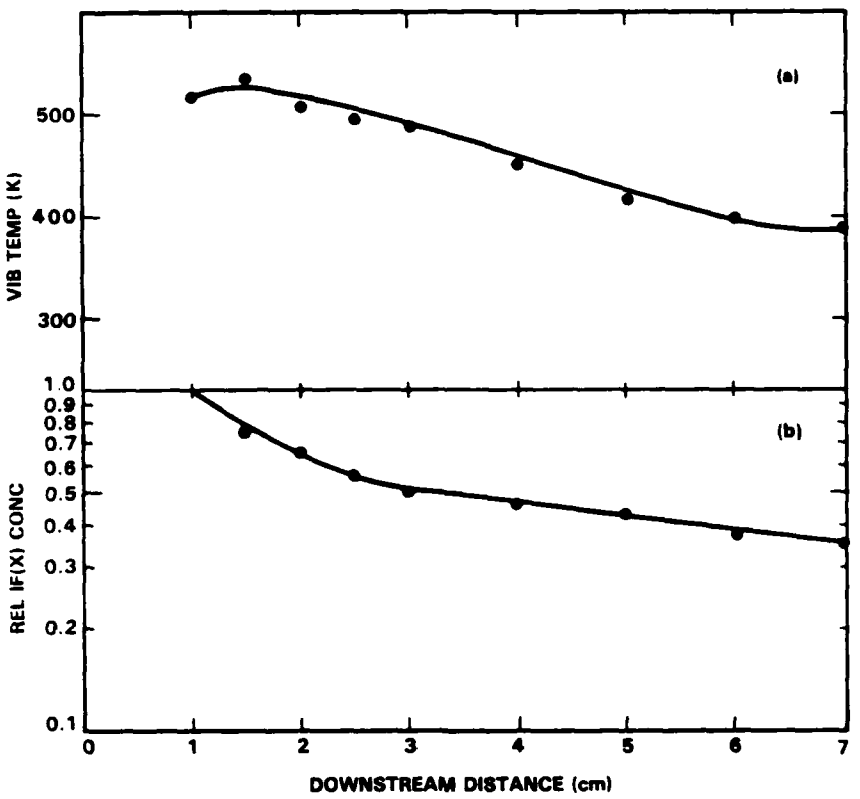

Fig. 9 Spatial distribution of the IF(X) vibrational temperature (a) and relative number density (b) downstream of the CF_3I injection. (These data were taken with initial F_2 and CF_3I concentrations of 170 and 24 mtorr, respectively. Total pressure was 656 mtorr.)

Several possible reactions may occur which could account for the initial rapid decay of the IF concentration by increasing the gas temperature or through chemical removal of the IF.

$$CF_3 + IF \rightarrow CF_4 + I \qquad (1)$$

$$CF_3 + CF_3 \rightarrow C_2F_6 \qquad (2)$$

$$CF_3 + F_2 \rightarrow CF_4 + F \qquad (3)$$

These reactions contribute approximately 30, 100, and 60 kcal/mole of exothermicity to the flow. Should reaction (1) be significant, removal of the CF_3 radicals by reactions (2) and (3) would account for the initial fast removal of IF followed by a slower removal rate since CF_3 radicals would be consumed.

The rotational temperature of IF(X), which is assumed to be the thermal temperature of the gases in the flow tube, can also be obtained using the LIF technique. The number density of a specific ro-vibrational level is given by the following relationship:

$$n_{v,J} = n_o \frac{(2J + 1)e^{-Bv'(J)(J + 1)/kT}}{Qrot} \quad \frac{e^{-Ev'/kT}}{Qvib} \qquad (4)$$

where the Q's are the associated partition functions and n_0 is the total IF(X) number density. Normalizing the LIF signal S for the laser power L, the following expression can be derived,

$$\ln \left[\frac{Sv''}{Lv'' (J + 1)} \right] = \ln C - \frac{Bv''}{kT} J(J + 1) \qquad (5)$$

where Sv" is the LIF signal strength and Lv" is the laser power. All J independent terms are lumped together in the proportionality constant C. Hence a semilog plot of the normalized LIF signal strength divided by the J+1 term (resulting from the R branch line strength formula) vs J(J+1) yields a slope whose absolute value is Bv"/kT. Such a plot was constructed and is presented in Figure 10. The data were obtained 2.2 cm downstream of the CF_3I injector. LIF signal strengths were recorded for the R(J) transitions of J = 9, 20, and 30. The slope of the line suggests a temperature of 550 K which is reasonable agreement with a vibrational temperature of 500 K even though the scatter in determining the rotational temperature is relatively

large. The agreement between the rotational and the vibrational temperature is not surprising, since the time scale for vibrational relaxation need be only on the order of ms for equilibration in the flow tube.

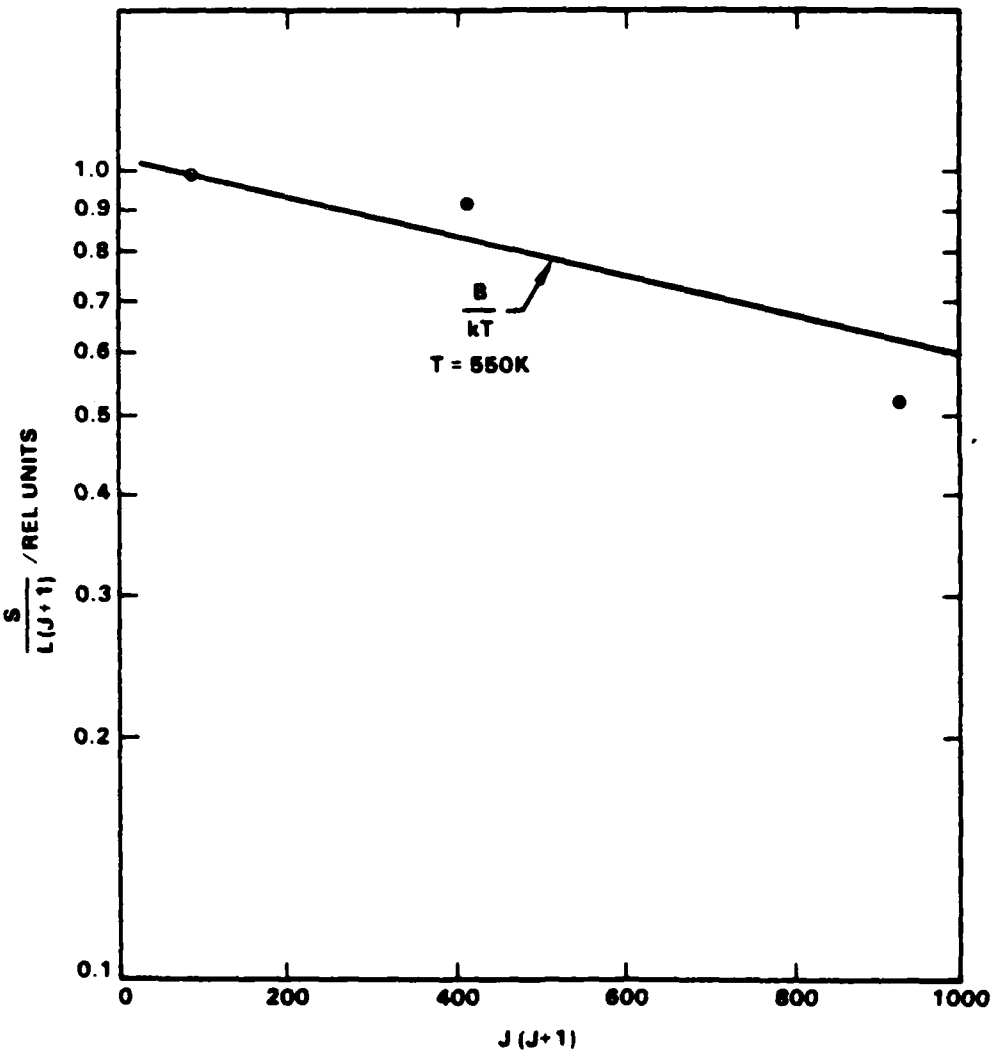

Fig. 10 Plot of normalized LIF signal strengths vs J(J + 1).

III. NF(b) GENERATION

Key to the success of this work was finding suitable means of generating the b state of NF. Several methods were attempted in the flow tube apparatus including both steady state and pulsed techniques. Common to all the techniques of generating NF(b) was the use of energy pooling reactions involving NF(a). For this work, NF(a) was generated in the following two-step reaction sequence (Ref. 18).

$$F + HN_3 \rightarrow HF(v\leq 5) + N_3 \qquad (6)$$

$$F + N_3 \rightarrow NF(a) + N_2 \qquad (7)$$

The exothermicity of the first reactions is sufficent to populate HF up to the v' = 5 level. As long as the F atom concentration is in excess, rapid reaction with the N_3 radicals results in a spin-constrained process yielding nearly 100% NF(a) (Ref. 19). The b state of NF is observed in these flames due to the pooling reaction,

$$HF(v>2) + NF(a) \rightarrow HF(v-2) + NF(b) \qquad (8)$$

Since only a small fraction of the exothermicity of reaction (1) is channeled into the higher vibrational levels of HF, only a small fraction of the NF(a) is converted to the b state as is observed by the relative emission strengths of the b-X and a-X bands. Typically, the concentration of NF(b) to that for NF(a) is of the order 0.01-0.03. Reaction (8) is nearly resonant with an equilibrium constant of 1. The rate of reaction (8) is thought to require

---

Ref. 18 R.D. Coombe and A.T. Pritt, Jr., Chem. Phys. Lett. 58, 606 (1978).

Ref. 19 A.T. Pritt, Jr., D. Patel, and R.D. Coombe, Int. J. Chem. Kinetics 16, 977 (1984).

only 1-10 gas kinetic collisions (Ref. 20); hence the NF(b) is held in equilibrium, having a lifetime determined by that of NF(a) and HF(v>2). Although the NF(a) decays rather slowly down the flow tube (having 1/e values corresponding to distances in excess of 10 cm), the HF(v) decays rapidly primarily due to the fast V-R,T rates known for HF self-quenching (Ref. 21). As the v>2 levels decay, so does the NF(b). Fortunately, the flames are bright enough so that reasonable signal-to-noise fluorescence signals can be obtained as far as 10 cm downstream from the point of reagent mixing.

In addition to using HF(v>2) as an energy pooling agent, the excited spin-orbit state of atomic iodine also converts NF(a) to NF(b). This energy pooling reaction,

$$I^* + NF(a) \rightarrow I + NF(b) \qquad (9)$$

has been observed by Herbelin and co-workers at the Aerospace Corp. (Ref. 22). Rockwell has also used this method of generating NF(b) in both steady-state and pulsed techniques. Flows of I* were generated by passing CF_3I or C_3F_7I through a quartz cell in which the output from a high intensity Hg capillary lamp was focused. It is well known that broadband photolysis in the UV (240 - 300 nm) fragments these iodine compounds to form I* (Ref. 23). Prior to introducing the photolyzed CF_3I to the flow stream, a fluorine atom scavenger such as CD_4 or D_2 was added to the flow downstream of the F + HN_3 reaction, but upstream of the point at which I* was added to the flow. Two pulsed methods of generating transient quantities of I* were attempted. The first pulsed method consisted of adding unphotolyzed CF_3I to the flow, as in the above case, and dissociating the CF_3I with a KrF excimer laser to generate

---

Ref. 20 M.A. Kwok, J.M. Herbelin, and N. Cohen, Electronic Transition Lasers (MIT Press, Cambridge, MA, L.E. Wilson, et al., eds., 1976) 8.

Ref. 21 J.T. Yardley, Introduction to Molecular Energy Transfer (Academic Press, Inc., New York, 1980).

Ref. 22 M.A. Kwok and J.M. Herbelin, Electronic Transition Laser II (MIT Press, Cambridge, MA, L.E. Wilson, et al, ed., 1977) 100.

a transient concentration of I*. The second pulsed method was to add either DI or I_2 to the flow stream and optically pump the iodine atoms generated by the F + DI reaction or the F + I_2 reaction with an I* photolysis laser. This second pulsed method is advantageous in that the excess fluorine atoms need not be scavenged. The details of each of these experiments, including their results, are reported in this section.

1. STEADY-STATE METHODS

The most readily available source of NF(b) is in the F + HN_3 reaction. This source, however, produces only a small fraction of NF(b). This limitation is due primarily to the small fraction of HF produced in the required v'> 2 levels. Sloan, et al (Ref. 24), has shown that the F + HN_3 reaction generates less than 20% of the HF in v'> 2. Since the V-T, R rate in HF is so efficient, the HF does not live very long down the flow tube for concentrations of HN_3 on the order of 1 mtorr; therefore, the lifetime of NF(b) is also short along the flow.

Since the concentration of NF(b) generated by the F + HN_3 flame is extremely small compared to the reagent concentrations, we sought to enhance its production by introducing a steady flow of I* to the flow tube reacting mixture. Recycling of IF(X) in the NF/IF energy transfer system may be observed if sufficient concentrations of NF(b) were generated. For these steady-state experiments, I* was generated by passing n-C_3F_7I through a quartz tube which was continuously illuminated by a high-pressure Hg arc capillary lamp (Universal Light Source, AH6-4BC). A schematic of the chemiluminescence flow tube apparatus, modified to accommodate the photodissociated n-C_3F_7I, is shown in Figure 11. Light from the lamp was reflected into the quartz tube by

---

Ref. 23 S.R. Leone, Adv. Chem. Phys. 50, 255 (1982).
Ref. 24 J.J. Sloan, D.G. Watson, and J.S. Wright, Chem. Phys. 43, 1 (1979).

a highly polished elliptical mirror block assembly, which was 10 cm long. The axes of the lamp and the quartz flow tube were positioned at the two axial foci.

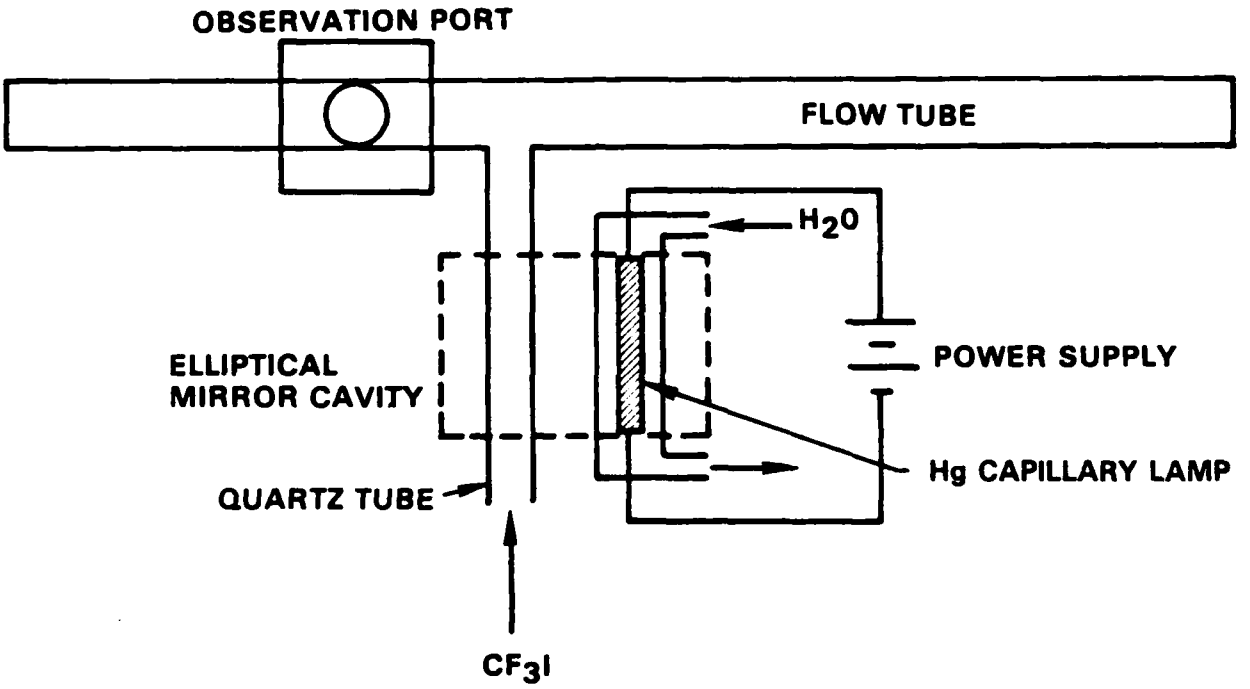

Fig. 11 Schematic of the CW photolysis experiment.

In these experiments, NF(a) was generated by the F + DN_3 reaction to avoid NF(b) production via vibrationally excited HF(v>2). Moreover, it is known that HF quenches I* much faster than does DF (Ref. 25). DN_3 was produced on-line in a manner similar to that for HN_3, using deuterated reagents, D_2SO_4 and D_2O. Prior to operation of the flow tube, the system was purged of hydrogen species by flows of D_2O vapor entrained in argon for

Ref. 25 A.T. Pritt, Jr. and D. Patel., J. Chem. Phys. 81, 1337 (1984).

approximately 20 h. DN_3 was added through the annular injector. Since the addition of undissociated n-C_3F_7I would generate IF by reaction with the excess fluorine atoms, thus removing NF(b) through the energy transfer reaction, D_2 was added to the central injector to quantitatively remove the fluorine atoms.

The F + DN_3 flame appeared light yellow due to the N_2 first positive emissions generated by the azide radical self-annihilation reaction (Ref. 26). Addition of D_2 resulted in much brighter yellow-orange flames due to the presence of D atoms produced in the F + D_2 reactions. The D atom reaction with NF(a) results in the following reaction sequence,

$$D + NF(a) \rightarrow DF + N(^2D) \quad (10)$$

$$N(^2D) + NF(a) \rightarrow N_2(A^3\Sigma_u^+, B^3\Pi_g) + F \quad (11)$$

The increased yellow-orange fluorescence is due to the latter reaction, producing more N_2 first positive emissions. The extent of this reaction in the flow tube is unknown, but we note that the reaction (10) is reported to be slow (Ref. 27). A small NF b-X emission signal was observed in the flame even with the photolysis lamp off. When the lamp was on and the power delivered was 1200 W, the NF b-X emission signal increased approximately sixfold. Integration of the NF b-X emission indicated that the absolute NF(b) concentration was 2×10^{11} cm^{-3}, whereas the estimated maximum NF(a) concentration was 10^{14} cm^{-3}. The addition of D_2 increased the decay rate of NF(a) as shown in Figure 12. Hence, with the central injector positioned upstream of the photolysis entrance, approximately 3% of the initial NF(a) was available for

---

Ref. 26 L.G. Piper, R.H. Krech, and R.L. Taylor, J. Chem. Phys. 71, 2099 (1979).

Ref. 27 C.T. Cheah and M.A.A. Clyne, J. Chem. Soc. (Faraday II) 76, 1543 (1980).

excitation to the b state at the point where I* entered the flow. The ratio of the NF(b) concentration to the NF(a) value was 0.07. Thus, the low value for the NF(b) was primarily limited by the available NF(a) in the flow.

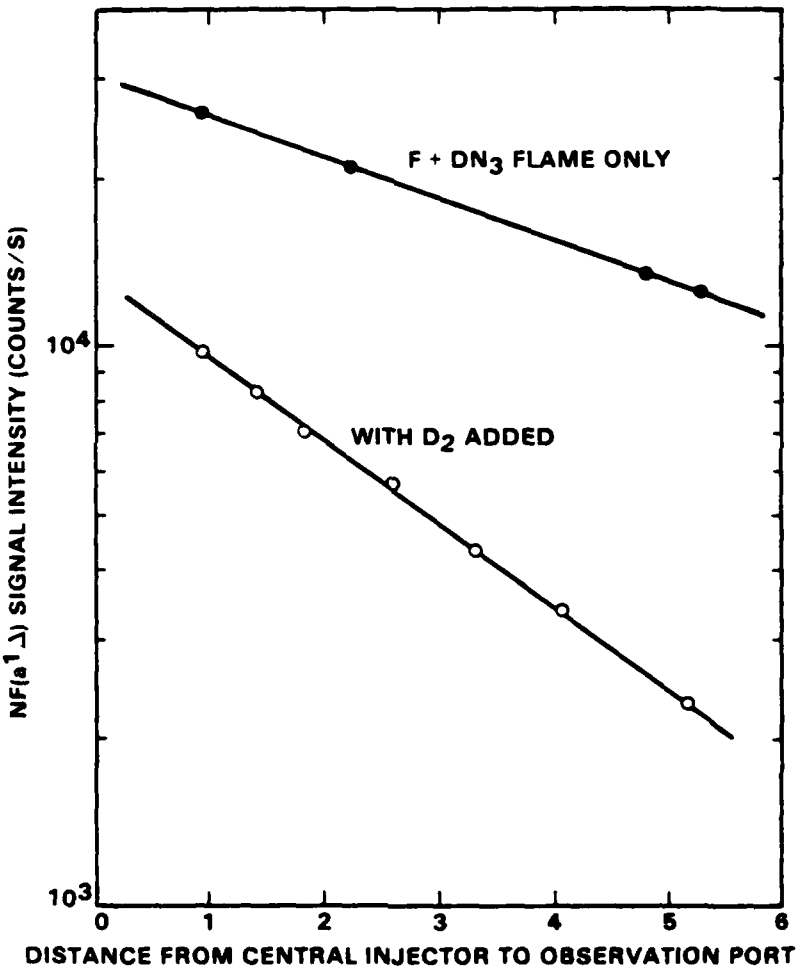

Fig. 12 Decay of the NF ($a^1\Delta$) in the F + DN_3 flame. (Approximately 27 mtorr of atomic fluorine was reacted with 24 mtorr DN_3. The enclosed circles refer to only the F + DN_3 flame, and the open circles to the case where 178 mtorr of D_2 was added to the flow.)

A rough calculation for the fraction of the n-C_3F_7I which was photolyzed suggested that, at most, 1% of the flow was dissociated. This calculation was based on a published spectral distribution of the lamp supplied by the manufacturer and assumed that all the light from the lamp was focused into the quartz flow tube. For these experiments, 200 mtorr of n-C_3F_7I was added to the flow yielding 2 mtorr of I*. Hence, the limiting reagent for reaction (4) would have been the NF(a).

Due to the rapid quenching of NF(a) by the addition of D_2 to the flow, CD_4 was used. A liter flask containing 1 atm of CD_4 was expanded into a 16-ℓ stainless steel ballast tank which had been previously passivated with 1 atm of D_2 for 24 h. Argon was then added until a total pressure of 928 torr was attained. The fraction of CD_4 in the mixture was 0.0584. Addition of the CD_4/Ar mixture to the F + DN_3 flame produced bright emissions which masked the NF a-X transition at 874.2 nm. To titrate the fluorine atoms, the CD_4/Ar mixture was added through the annular injector while DN_3 was added through the central injector 5 cm downstream. The flow of CD_4 was increased until the F + DN_3 flame was extinguished, thus quantitatively removing all the fluorine atoms from the flow. The order of the reagents was reversed: the DN_3 added upstream through the annular injector, and the CD_4 mixture added downstream through the central injector. Flows of n-C_3F_7I diluted in argon were then passed through the photolysis region. An approximately sixfold enhancement of the NF b-X emission was observed, the same as found when D_2 was used as the fluorine atom scavenger. The steady-state method of generating NF(b) was therefore abandoned since the concentration of NF(b) generated was less than that which could be produced in the usual F + HN_3 flame.

2. PULSED METHODS FOR GENERATING NF(b)

The first method attempted for producing transient concentrations of NF(b) was to use a KrF excimer laser to photodissociate CF_3I. As in the steady-state method, excess fluorine atoms needed to be removed prior to the

addition of the perfluoroalkyliodide to prevent formation of IF which would rapidly quench NF(b). For these experiments, we again used the CD_4/Ar mixture and titrated the fluorine atoms, as described in the CW photolysis experiments. Pure unphotolyzed CF_3I was added through the same port that the n-C_3F_7I was added in the CW photolysis technique. The KrF laser beam was passed through the CaF_2 window located at the downstream end of the flow tube and was steered coaxially up the flow tube. The emissions from the observation port were dispersed by the 1-m spectrometer system, but the photoelectric pulses were sent to the MCS input of the Nicolet 12/70 signal averager. The signal averager was triggered by the synchronous output pulse from the excimer laser. The channel width was set to 10 μs, which would result in accumulating approximately 20 counts per channel per laser firing if the concentration of NF(b) was on the order of those obtained in the F + HN_3 flame. After ten averages, no emission of NF(b) was observed for these experiments. When the flow of CD_4/Ar was stopped and the flow of CF_3I was continued, no NF a-X emissions were observed. Hence, NF(a) was quenched efficiently by the CF_3I or by the products of the F + CF_3I reactions. With no detectable amounts of NF(a) in the flow tube, all attempts at generating I* by pulsed photolysis of CF_3I were stopped.

A commercial dye laser (Phase-R, Model 2100A) was converted to gas operation by modifying the flash lamp assembly as prescribed by the manufacturer. The laser was converted to an I* photolysis laser by forming an optical cavity around the laser, consisting of a 100% flat reflector at 1.3 μm and a 50% output flat mirror. With approximately 150 torr of CF_3I flowing through the laser cavity and with a discharge of 242 J of energy through the flash lamp, an I* laser energy of approximately 20 mJ was measured by a Gentec energy meter.

In the flow tube, DN_3 was added through the annular injector. A liter flask of 1 atm DI (Merck, Sharpe, and Dome) was transferred to the saturator (196 K) through which argon was passed at a regulated pressure. The fraction of DI, as measured by monitoring its UV absorption at 250 nm in the

mixture, was typically 0.35. The mixture was added to the flow tube through the central injector. The central injector was positioned one cm upstream of the observation port. Prior to the addition of DI, about 40% of the DN_3 added to the flow resulted in the production of NF(a) as determined by photon calibration of the spectrometer at 874.2 nm using the O + NO chemical actinometry technique (Ref. 14). Addition of approximately 20 mtorr of DI reduced the NF(a) concentration by a factor of 4. Furthermore, second overtone emissions from HF(v=3) were observed. The presence of vibrationally excited HF in the flow tube indicated that the DI was contaminated with some hydrogen-bearing species, undoubtedly HI.

The output from the I* laser was passed through the reacting mixture in the same manner as was done in the KrF excimer laser experiments. The intensity of the emission signal at 529 nm, as shown in the time trace of Figure 13, was linear in both the concentration of DI added to the flow and the power of the I* laser. Decreasing the dwell time per channel to 2 μs, which is the fastest time allowable for the signal averager, resulted in an improvement of the time resolution of the traces. The slit width of both the entrance and exit ports of the monochromator was set to 1 mm to enhance the signal strength.

Based on the data collected in Figure 13, an estimate for the energy pooling reaction (9) could be obtained and compared to the value reported by Herbelin and Kwok (Ref. 28). To determine the pooling reaction rate constant, the initial concentrations of NF(a) and I* must be estimated. Hence, the resulting rate constant determined would reflect the uncertainties of these initial estimates. For the data shown in Figure 13, the initial partial pressures for the F atoms, DN_3, and DI were 32.5, 3.1, and 4.0 mtorr. From an earlier study, we discovered that the fraction of HN_3, which is converted to

---

Ref. 28 J.M. Herbelin and M.A. Kwok, Electronic Angular Momentum Transfer in the $I(^2P_{1/2})$ + NF(a'Δ) System, SAMSO-TR-76-62, The Aerospace Corporation, El Segundo, CA (1976).

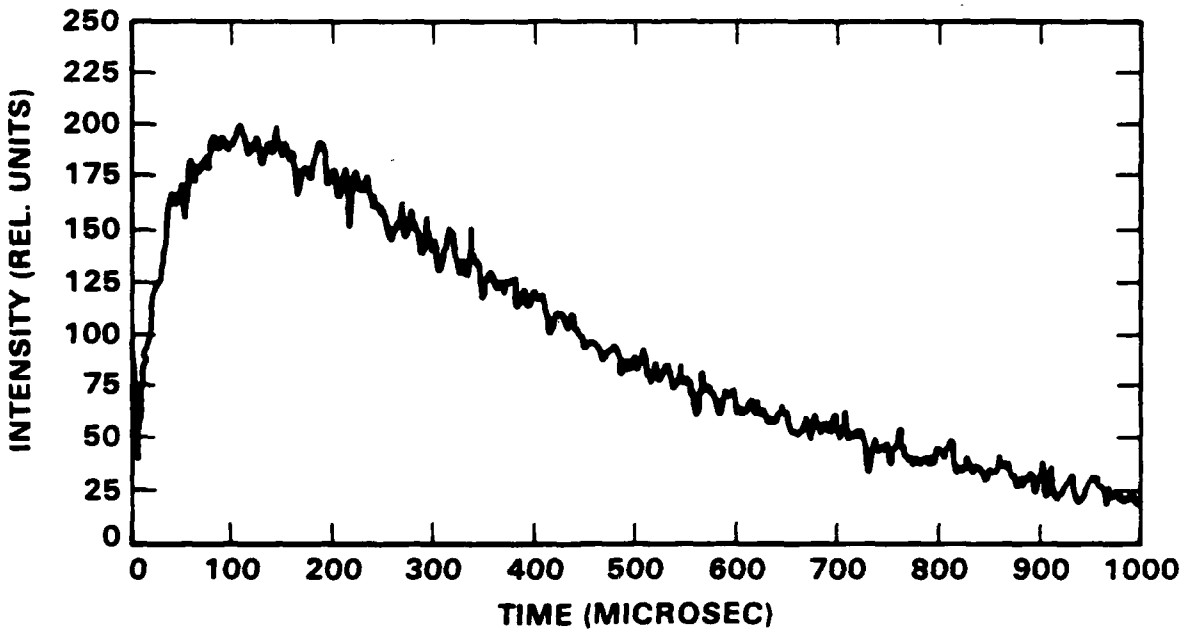

Fig. 13 Temporal profile of the NF b-X emission following pulsed optical pumping of atomic iodine in the presence of NF(a).

NF(a) under these conditions, would be 0.25. Given the power of the laser, we estimate that 0.06 of the total iodine atoms were pumped to I*. Based on these values, the pooling reaction was numerically fitted to the data shown in Figure 13. The rate constant, which best fit the data, was 2.4×10^{-10} cm^3/molecule/s. This value can be compared to the reported value of 4.3×10^{-10} cm^3/molecule/s. The reported pooling rate constant depended on the value of the spontaneous radiative rate of NF(a). Subsequent work (Ref. 29) led to a reevaluation of the NF(a) radiative rate. The rate constant, therefore, must be adjusted downward by a factor of 5.6. Making this adjustment and considering that the value for the pooling reaction rate constant is, at best, within a factor of 4 of the actual value, we can state that the observed rise in the NF b-X fluorescence in Figure 13 is in accordance with the reported energy pooling rate.

Ref. 29 R.J. Malins and D.W. Setsen, J. Phys. Chem. 85, 1342 (1981).

IV. E-E ENERGY TRANSFER RATE CONSTANT, k*

As reported earlier, IF(B) in the F + HN_3 + I_2(CF_3I) flame is present only in the company of NF(b), leading to the conclusion that the production of IF(B) is through an E-E energy transfer process. This section presents a method for measuring the E-E energy transfer rate constant. The rate constant is then presented as a function of the fluorine atom concentration and the vibrational distributions of NF(b) and IF(B). Since the rate constant increases as the fluorine atom concentration decreases, interference effects from second order reactions occurring in the F + HN_3 reaction were suspected as a possible second path for the production of IF(B). This confuses the origin of the observed IF B-X emissions. Two separate experiments were developed to verify that the source of IF(B) in these flames was indeed due solely to E-E energy transfer processes from NF(b). Finally, the rate constant was measured as a function of the vibrational distribution of IF(X) in the flow tube, using the LIF diagnostic described in an earlier section.

Assuming that the source of IF(B) in the F + HN_3 + RI flames is due to an E-E energy transfer process involving NF(b) as the energy transfer agent, the steady-state concentration for a given v' level for IF(B) at each point in the flow is related to the E-E energy transfer rate constant k* as follows:

$$[IF(B)] = k^*[NF(b)][IF(X)]/A_B \qquad (12)$$

where A_B is the radiative rate of the IF(B). It is assumed that the radiative rate is much faster than any collisional removal processes in Eq. (12). Given that the reagent partial pressures are on the order of a few mtorr, removal of IF(B) through bimolecular collisions with these reagents would be unlikely, even if the quenching efficiency approached unity. The radiative rate of 1.4×10^5 s^{-1} is much faster than the rate at which the gases flow down the

flow tube, and much faster than the rate at which IF(B) is formed in the E-E energy transfer process. Hence, we make the assumption that as soon as IF(B) is formed, it radiates and, therefore, is detected by the spectrometer system. The measured signal, therefore, is

$$S_{IF(B)} = T(\lambda)G\ A_B\ k^*[NF(b)][IF(x)]/A_B \qquad (13)$$

where $T(\lambda)$ is the relative wavelength dependent response of the 1-m spectrometer, and G is a geometric constant representing the fraction of the total photon flux which is dispersed and detected by the spectrometer. Similarly, the concentration of NF(b) can be determined as follows:

$$[NF(b)] = \frac{S_{NF(b)}}{T(\lambda)G\ A_b} \qquad (14)$$

where A_b (= 45 s^{-1}) is the radiative rate of the b state of NF (Ref. 30). Substituting Eq. (14) into Eq. (13) and solving for the rate constant yields the following expression:

$$k^* = A_b(S_{IF(B)}/S_{NF(b)})/[IF(X)] \qquad (15)$$

Ref. 30 P.H. Tennyson, A. Fontijn, and M.A.A. Clyne, Chem. Phys. 62, 171 (1981).

Since only a portion of the total IF(B) spectrum is taken (typically from 450-600 nm), the rate constant for populating each v' level of the B state is determined as follows:

$$k_{v'} = \frac{A_b}{[IF(X)]} \frac{\left(\frac{\langle \nu_{v'} \rangle}{\nu_{v',v''}}\right)^3 \int \frac{S_{IF(b,v'-v'')}}{T(\lambda)\, q\,(v'v'')}\, d\lambda}{\int \frac{S_{NF}\,(b,\, o-o)}{T\,(523\ nm)\, q\,(o,o)}\, d\lambda} \qquad (16)$$

where the integrals are taken over the selected v'-v" band, and q(v',v") is the associated Franck-Condon factor for the respective transitions (Ref. 31). Thus, the total rate constant is $k^* = \Sigma\, k_{v'}$. The bands used to determine each $k^*_{v'}$ were the 0-4, 1-3, 2-2, 3-1, 4-1, 5-0, 6-0, 7-0, and 8-0. These selected bands have the least overlap with other emitting bands, as can be observed in a typical spectrum shown in Figure 6.

The IF(X) concentration is also required in Eq. (16). Since IF(X) is a transient species, the LIF diagnostic was used to monitor its relative concentration along the flow tube (see Figure 9). For most applications, the concentration of the IF(X) used in the above equation was simply taken as that initial concentration of the iodine bearing species added to the flow tube. When measurements were made far downstream of the RI injection point, the determination of k* must include the decay of IF(X). At most, the rate constant would be adjusted upwards by a factor of 2.

To determine the E-E energy transfer rate constant, spectra were taken in the 450-600 nm region. In addition, the flow rates of all the gases were monitored, and the fraction of HN_3 and RI components were determined from the UV absorption data. From these flow rates and the total pressure in the flow tube, the partial pressure of each of the reagent flows was determined. The F atom partial pressure was determined via the Cl_2 titration technique

Ref. 31 K.A. Mohamed, B.N. Khanna, and K.M. Lal, Ind. J. Pure Appl. Phys. 12, 243 (1974).

(Ref. 32), in which Cl_2 was continuously added to the flow and the Cl_2 recombination emissions (Cl_2 B-X transition) were monitored. The recombination fluorescence showed a marked quadratic dependence on the Cl_2 flow rate until all the F atoms were consumed, at which point the Cl_2 recombination fluorescence remained constant. The Cl_2 flow rate corresponding to this endpoint, therefore, represents the original F atom concentration. It was found, however, that as long as the microwave discharge was tuned to its minimum reflectance power from the Evanson cavity, 50% of the molecular fluorine was dissociated for all flows of F_2 used in this work. Consequently, the F atom flow rate was assumed to be equal to the molecular fluorine flow rate (two fluorine atoms are generated for every F_2 dissociation) even though the Cl_2 titrations were not done for every determination of k*.

1. k* VS THE FLUORINE ATOM CONCENTRATION

Earlier, the E-E energy transfer rate constant was found to depend linearly on the concentration of I_2 added to the flame (Ref. 10). However, we discovered that, as the fluorine atom concentration was decreased, the rate constant, as determined by Eq. (16), increased. The rate constant was determined, assuming that the IF(X) concentration was equal to the initial concentration of CF_3I added to the flow stream. A plot of the rate constant, reported in terms of $torr^{-1}s^{-1}$ since the flame temperature was unknown, is plotted against the fluorine atom concentration. The fluorine atom concentration was taken as the remaining F atom concentration after complete reaction with CF_3I. For these data, CF_3I was added through the annular injector 1 cm upstream of the central injector through which HN_3 was added. The chemiluminescence was observed approximately 1 cm downstream of the central injector.

As noted in Figure 14, the value of the E-E energy transfer rate constant increased as the fluorine atom concentration was reduced for constant

---

Ref. 32 P.S. Ganguli and M. Kaufman, Chem. Phys. Lett. 25, 221 (1974).

CF_3I and HN_3 flows. This result suggests that either the gas temperature changed or that an alternate path for generating IF(B) began to dominate. Consider the following reactions,

$$F + HN_3 \rightarrow HF(v) + N_3 \quad (17)$$

$$F + N_3 \rightarrow N_2 + NF(a) \quad (18)$$

$$N_3 + N_3 \rightarrow N_2(A) + 2N_2 \quad (19)$$

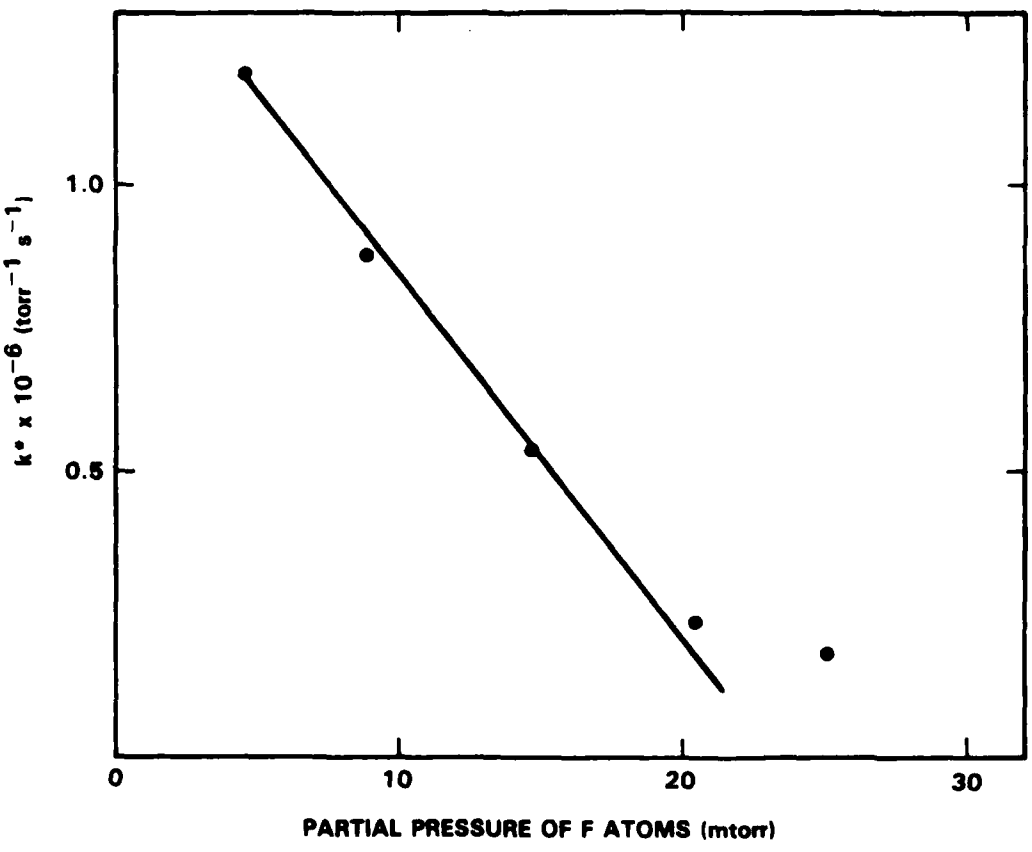

Fig. 14 Plot of the E-E energy transfer rate constant as a function of the partial pressure of fluorine atoms.

Since the rate constant for reaction (17) is 1.3×10^{-10} $cm^3/molecule^{-1}/s^{-1}$ (Ref. 33), while that of the second reaction is 2×10^{-12} $cm^3/molecule^{-1}/s^{-1}$ (Ref. 34), an intermediate concentration of N_3 is formed. If the fluorine atom concentration is sufficiently large, the disappearance of N_3 is primarily via reaction (18). However, as the concentration of F atoms is reduced, the second-order reaction (19) begins to dominate. Piper, et al[†], have shown that $N_2(A)$ rapidly transfers its electronic energy to IF(X), forming the B state. Consequently, the apparent increase in k*, shown in Figure 14, may be due to the increased formation of $N_2(A)$. This analysis would seem to explain the data; however, the intensity of the IF B-X emission did not increase as the F atom concentration was reduced. The increase in the value of k* stems primarily from the decrease in the NF b-X emission intensity. This latter factor would tend to suggest that any decrease in the formation of IF(B), due to the decrease of NF(b), was directly offset by the increase in the production of IF(B) via the $N_2(A)$ pumping scheme. Alternative explanations may center on changing conditions (e.g., temperature) in the flow tube as the F atom concentration is decreased. The vibrational temperature associated with the b state of NF also increases with decreasing F atoms. In analyzing the B-X emission bands for the relative populations of the v' levels in the product IF(B), the distribution appears Boltzmann, and this vibrational temperature increases as the F atom concentration is decreased. The greater vibrational temperatures of the product IF(B) may represent the change of not only the vibrational distribution within the b state manifold of NF, but also changes in the vibrational distribution of the X state of IF.

[†]L.G. Piper, PS Inc., presented at the SWCL Workshop, Charleston, SC., November 15, 1984.

Ref. 33 A.T. Pritt, Jr., Excited State Chemistry of Halogen Azides, AFOSR Report No., AF Office of Scientific Research, Bolling AFB, DC (1982).

Ref. 34 A.T. Pritt, Jr., and R.D. Coombe, Int. J. Chem. Kinetics 12, 743 (1980).

2. k* VS THE VIBRATIONAL DISTRIBUTION OF NF(b)

Assuming that the bulk of the IF B-X chemiluminescence stems from the E-E energy transfer from NF(b) to IF(X), we have correlated the observed k* data with the vibrational distribution of NF(b). A semilog plot of the E-E energy transfer rate constant is plotted vs the reciprocal vibrational temperature of NF(b) in Figure 15. Although the data tend to follow a trend of increasing k* with increasing vibrational temperature in NF(b), the scatter is large, showing multiple values of k* for a given vibrational temperature of NF(b).

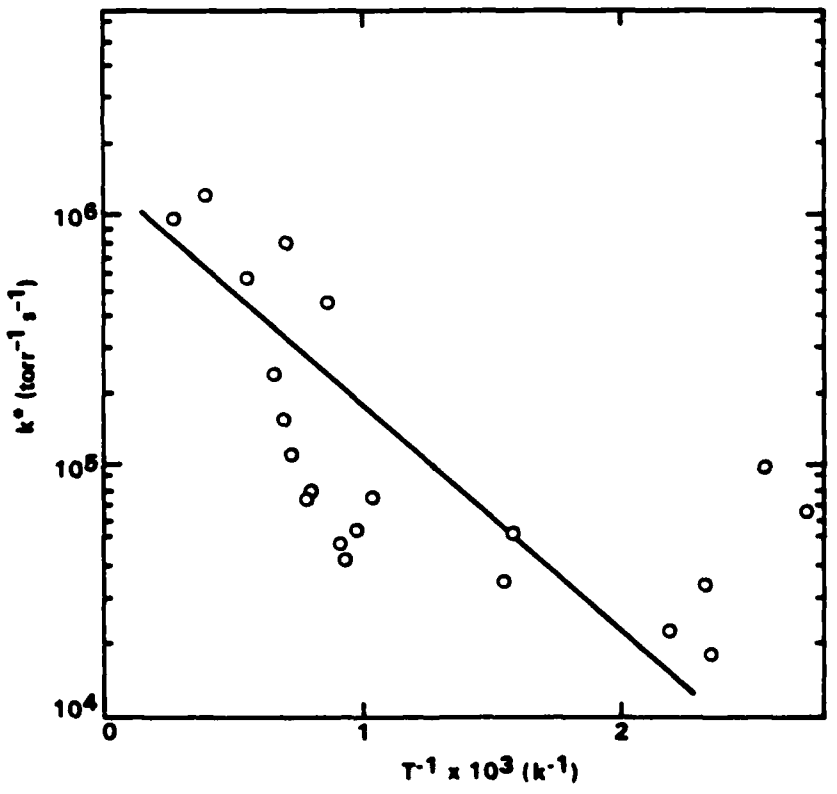

Fig. 15 Arrhenius plot of k* vs the reciprocal vibrational temperature of NF(b).

3. k* VS THE VIBRATIONAL DISTRIBUTION OF IF(B)

The vibrational distribution of IF(X) is unknown for the data presented in Figure 15. If we make the assumption that the vibrational distribution in IF(B) is proportional to the vibrational distribution of IF(X), a plot of k* vs the reciprocal vibrational temperature of IF(B) may show a correlation between the observed value of k* and the IF ground state vibrational temperature. This plot is shown in Figure 16. This plot shows a strong correlation between increasing values for the vibrational temperature of IF(B) and with increasing values of the measured E-E energy transfer rate constant. Unfortunately, this correlation does not help define the source of excitation of ground state IF to the B state. The lack of correlation of k* with the vibrational distribution of NF(b) suggests that NF(b) may not be responsible for the observed IF B-X chemiluminescence. Hence, our work in this program was directed toward determining conclusively the source of the IF B-X chemiluminescence in the F + HN_3 + RI flames.

4. VERIFICATION EXPERIMENTS

Subsection (IV.1) noted that one possible explanation for the variation of k* may stem from possible E-E energy transfer processes involving $N_2(A)$ produced in the N_3 self-annihilation reaction (19). Hence, we sought to design experiments which would definitively establish the processes responsible for the observed IF B-X emission in the F + HN_3 + RI flames. Two experiments were devised.

In the first experiment, small amounts of NO were added to the flow stream to observe any NO γ band emissions which would be generated by the well-known efficient E-E energy transfer process,

$$N_2(A) + NO \rightarrow N_2(X) + NO(A) \qquad (20)$$

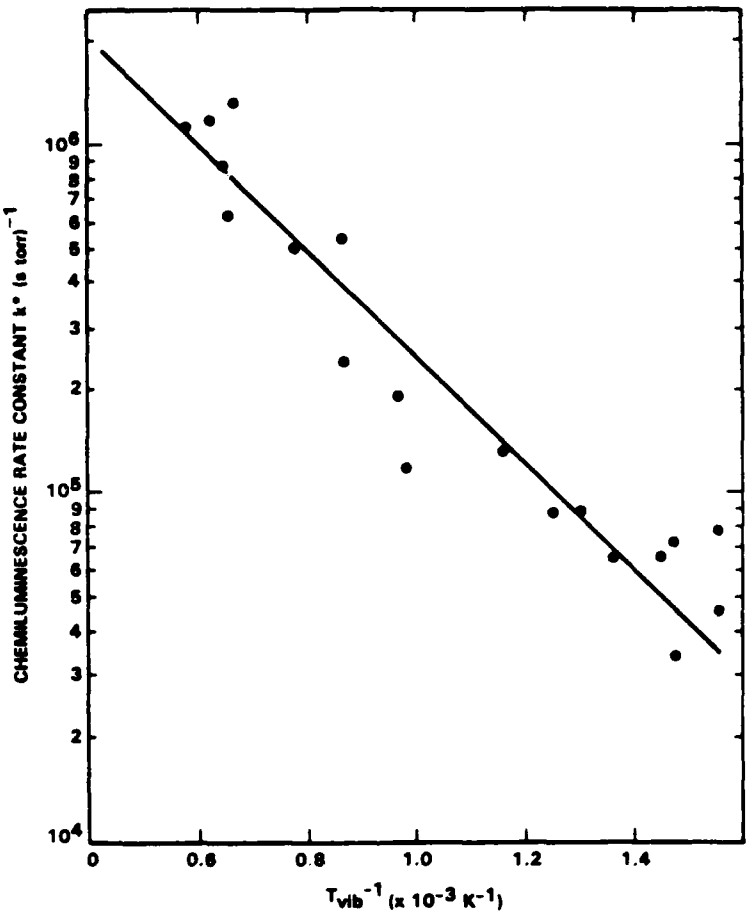

Fig. 16 Arrhenius plot of k* vs the reciprocal vibrational temperature of IF(B).

An NO/argon mixture was added upstream of the point where HN_3 and I_2 joined the flow stream. The γ band emissions occurred only when the F and HN_3 were reacted. The fluorine atom concentration was lowered to favor the azide radical self-annihilation reaction relative to the F + N_3 reaction which produces NF(a). The intensity of the NO γ bands increased more than sixfold, but the intensity of the IF(B) increased only by a factor of 2. The intensity of the NF b-X emission showed no change between these two sets of spectra. The data reveal that the sixfold increase of the NO γ band, which represents a sixfold increase in the $N_2(A)$, was not reflected in the intensity of the IF B-X intensity. The observed factor of 2 increase in the IF B-X emission could be explained in terms of the increased vibrational temperature in IF(X).

Although the above experiment is compelling evidence for NF(b) as the primary transfer agent for populating IF(B), the following experiment provides the final proof.

In this experiment, transient concentrations of NF(b) were generated by optically pumping atomic iodine to its excited spin-orbit state in the presence of NF(a). An I* photolysis laser was propagated through the downstream window coaxial to the flow tube. The distance between the annular and central injector was set to 8 cm. HN_3 was introduced through the annular region and I_2 was added to the flow through the central injector. The entire injector tube assembly was positioned 1 cm upstream of the observation port. It was noted that quenching of NF(a), by the addition of either CF_3I or I_2, resulted in an acceleration of the NF(a) decay down the flow tube; hence, the injector was placed as close to the observation window as possible to still provide reasonable mixing of the IF in the flow tube.

The slits of the spectrometer were set at 2 mm, and the wavelength to the peak intensity at the 0-0 band of the NF b-X emission. The output from the scaler was directed to the Nicolet 12/70 signal averager to record the transient fluorescence of NF(b) produced in the I* + NF(a) pooling reaction. Figure 17 shows the temporal response of the detector immediately following optical pumping of the flow mixture by the I* photolysis laser. From an estimation of the initial NF(a) and I* concentrations in the flow tube, the rise rate corresponds to the rate of the energy pooling reaction. The spectrometer was set to the 0,3 and 1,4 bands of the IF B-X emission whose temporal profiles are also shown in Figure 17. The fact that the IF B-X emission tracks the NF b-X emission is proof that these emissions are related to each other, and therefore demonstrates that NF(b) transfers its energy to IF(X) to form IF(B). At this point, it was necessary to determine the magnitude of the NF(b) E-E energy transfer rate to ascertain its importance in the previously observed chemiluminescence flames.

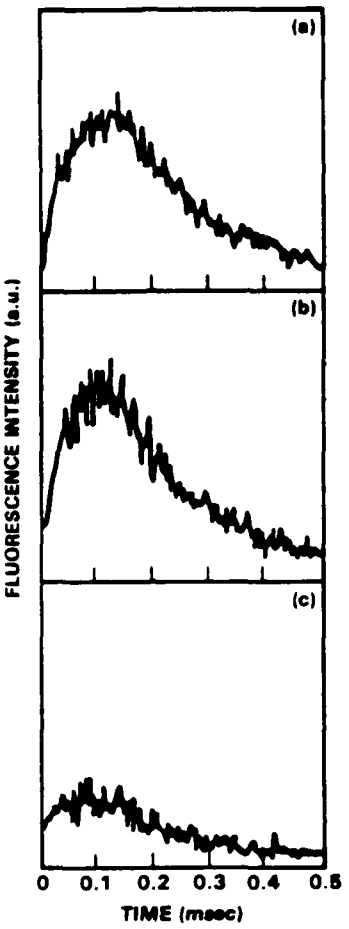

Fig. 17 Time profiles of selected NF(b) and IF(B) emissions following I* laser optical pumping.

Transient spectra were obtained using an optical multichannel analyzer (OMA), which was gated to its "on" condition during the most intense portions of transient emissions. Unfortunately, the sensitivity of the OMA system did not permit closing the aperture of the entrance slit to a point where the vibrational bands of the NF b-X emission could be resolved. Spectral resolution of the IF B-X bands, on the other hand, was easily obtained. For spectra taken by the OMA, the flows of the reagent gases were adjusted to maximize the intensity of the emissions. Spectra were taken with and without the laser beam blocked from the flow tube. A typical spectrum is shown in Figure 18. The difference spectrum, therefore, represents only those emissions due to optical pumping of the reacting mixture. The intensity of the difference spectrum was equal to or less than the intensity of the background

fluorescences. Care was taken to insure that the background fluorescence did not change between those experiments in which the beam was blocked and those in which the beam was unblocked, thus reducing any distortion of the difference spectrum. To insure constant emission strengths, the scaler used to monitor a given spectral component, usually the 0-0 band of the NF b-X emission, was monitored. If the emissions changed by less than 5%, the spectral data in the OMA was considered acceptable, since the signal was greater than 25% of the background signal. For some of these pulsed experiments, the NF(b) vibrational distribution temperature of the background fluorescence was determined, using the 1.0-m spectrometer system. The vibrational temperatures were typically 450-640 K.

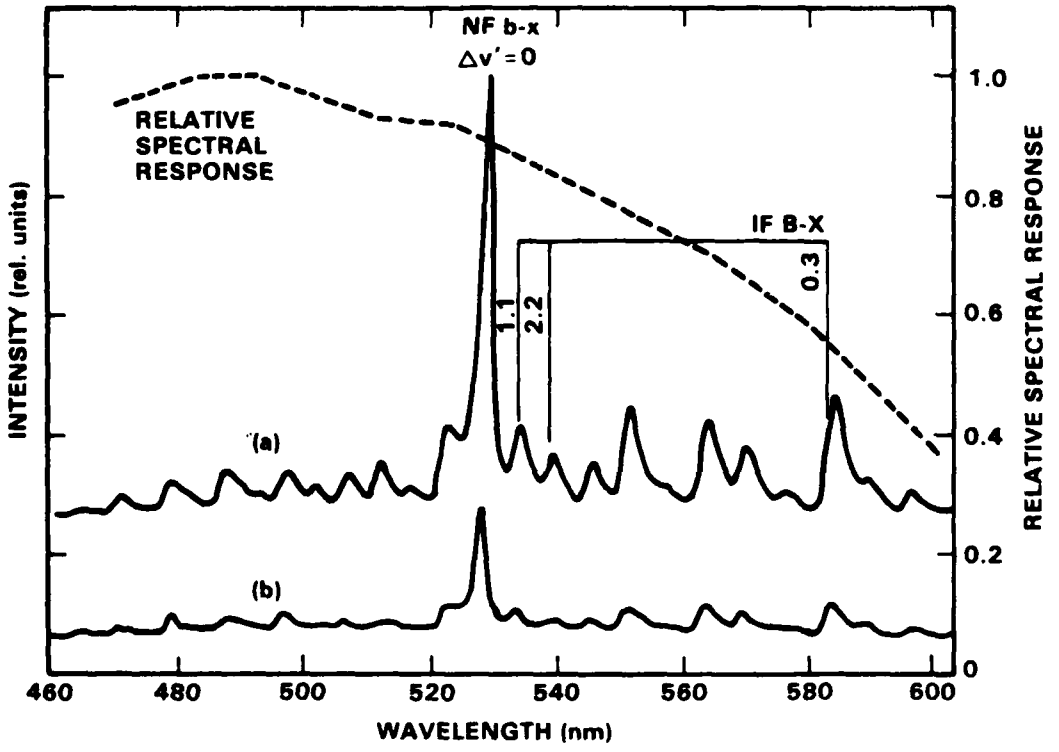

Fig. 18 Relative spectral response and spectra taken on the optical multichannel analyzer.

From the flow rate data and the spectrum obtained by the OMA spectrometer system, the energy transfer rate constant and the vibrational distribution of the emitting IF(B) were determined. The integrated band intensities were corrected, according to the spectral response of the OMA spectrometer system (as shown Figure 18), the cube of the bandhead frequency, and the appropriate Franck-Condon factor according to Eq. (16), thus generating a quantity proportional to the number density of the v' emitting B state of IF. The bands used to determine the vibrational distribution were the 0-3, 1-1 and 2-2. The sum of the integrated band intensities, which includes the Franck-Condon factor, was compared to the integrated intensity of the unresolved $\Delta v = 0$ progression of the NF b-X transition for determining the total chemiluminescence rate constant (see Eq. (16)).

For each experimental condition, the rate constant and the vibrational distribution were determined for both the background fluorescence of the flame and for the pulsed fluorescence generated by optically pumping the reacting mixture by the I* laser. These results are compared in Table 2. The agreement between the results obtained from the background fluorescence and those obtained from optical pumping suggests that the initial condition for both experiments was the same. This result is not surprising since the only difference between the two experiments was the method of generating NF(b). In both cases, NF(b) was generated via an energy pooling reaction with NF(a) and with HF(v>2) or I*. Since the v=2 energy in HF is nearly resonant with the spin-orbit energy of atomic iodine, the vibrational temperatures in the product, NF(b), for both energy pooling reactions are likely equivalent. Furthermore, the vibrational distribution in IF(X) is likely to be unaltered by the transient presence of I*.

The range over which the rate constant and the vibrational temperatures vary in the pulse experiments is more limited than in the previous steady-state experiments. These limitations stem from the low signal-to-noise obtained in the pulse experiment. For this reason, large flows of DN_3 were necessary to generate sufficient quantities of NF(a) for the energy pooling

TABLE 2

COMPARISON OF THE RESULTS FROM THE PULSED AND BACKGROUND FLUORESCENCE IN THE F + DN_3 + I_2 REACTION

Partial Pressure (mtorr)			Pulsed		Background	
F	DN_3[a]	I_2	T(K)	k*($torr^{-1}s^{-1}$)	T(K)	k*($torr^{-1}s^{-1}$)
39	21	1.8	790	267,000	849	361,000
18	19	1.9	1,639[b]	248,000[b]	920	773,000
27	18	2.3	339[b]	167,000[b]	956	352,000
32	20	2.3	542	191,000	787	354,000
41	17	2.3	595	324,000	686	316,000
32	18	2.2	746	438,000	800	464,000
24	18	2.3	710	304,000	817	448,000
35	16	2.3	635	621,000	738	530,000

[a]These values are only approximate, due to the inaccuracies of measuring the strong UV absorption in the DN_3 flow.
[b]These results are based on extremely poor signal/noise data for the pulsed fluorescences.

reaction. The I_2 flow rates were also maximized. Hence, the only reagent flow which could be adjusted to vary the temperature was that of F_2 (i.e., the F atom flow rate). The other adjustable parameter was the distance between the injector tube assembly and the observation port. In the steady-state experiments, generally the greater this distance, the lower the value for both the energy transfer rate constant and the vibrational temperature of IF(B). In the pulsed experiments the distance between the I_2 injector and the observation port could be varied between 2-3 cm. Positioning the I_2 injector any closer than 2 cm resulted in increased background fluorescence, increasing the error in the difference spectrum. Positioning the I_2 injector beyond 3 cm from the observation port produced such weak fluorescence that the error in determining the rate constant and the vibrational temperature was unacceptably large.

An Arrhenius plot of the data in Table 2 (the energy transfer constant log vs the reciprocal of the vibrational temperature of IF(B)) is shown in Figure 19. This plot can be compared to the earlier Arrhenius plot (see Figure 16), which was obtained from the steady state experiments. Although the scatter of the data is larger than those for the steady state experiments obtained earlier, the same correlation is exhibited. More vibrational energy observed in the IF(B) state corresponds to increased values for the E-E energy transfer rate constant. For the steady-state experiments, the total pressure in the flow tube was on the order of 800-900 mtorr. For the pulsed experiments, the pressure of the flow tube was typically greater than 1200 mtorr. Hence, the cooler vibrational temperature observed for IF(B) for equivalent transfer rate constants may be due in large part to increased vibrational relaxation prior to emission. For both sets of experiments, the rate constants lie primarily in the range of 10^5-10^6/torr^{-1}s^{-1}. Two basic conclusions can be drawn from the pulse experiments. First, NF(b) transfers its electronic energy to ground state IF, producing the excited B state in IF; and second, the energy transfer process observed under the pulsed conditions, which can only be attributed to NF(b) E-E energy transfer, occurs at a rate which accounts for all the observed B-X emissions in the steady-state chemiluminescence flames, even under conditions in which the fluorine atom concentration is reduced.

5. E-E ENERGY TRANSFER RATE CONSTANT AS A FUNCTION OF THE VIBRATIONAL DISTRIBUTION IN THE REAGENTS

From the previous section we now know that, with variations of the F atom concentration, the intensity of the IF B-X transition can be totally accounted for by energy transfer from NF(b). Since the resolution of the 1-m spectrometer is much greater than that for the OMA system, E-E energy transfer rate constants were determined using the direct chemiluminescence from the F + HN_3 + CF_3I flame. In addition to the spectral data, LIF was used to determine the vibrational and rotational distributions of the IF(X). After discovering that the rotational temperature roughly matched the vibrational temperature,

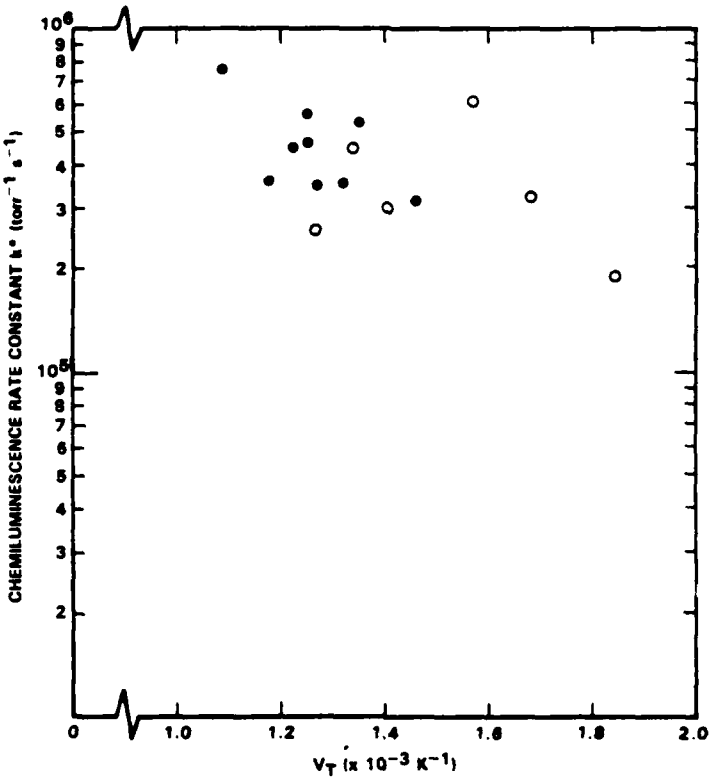

Fig. 19 Arrhenius plot of k* vs the reciprocal vibrational temperature of IF(B) determined from spectra taken on the OMA.

rotational distribution data collection was stopped. To vary the vibrational distributions in the two reagent molecules, NF(b) and IF(X), the fluorine atom concentrations were varied as in the earlier experiments.

The vibrational distribution of IF(X) was determined from the intensity of the LIF signal normalized to the laser power for two ro-vibrational lines. The dye laser was operated using Rhodamine 110, which can pump v"=1 and v"=2 lines. The LIF signals were recorded for the R(30) transition in the 1-1 and 1-2 bands. Since the same ro-vibrational level was accessed for both transitions, the LIF intensity distributions remained the same and no correction for the emission was necessary. Hence, the vibrational temperature was determined as follows:

$$T_{VIB} = \frac{E}{k}\left[\ln\left(\frac{S_1}{L_1 q_1}\right)\left(\frac{L_2 q_2}{S_2}\right)\right] \qquad (21)$$

where the S's are the strengths of the LIF signal, q's are the Franck-Condon factors, L's are the laser powers, E the energy separation between the two bands, and k the Boltzmann constant.

The E-E energy transfer rate constant was determined as previously described using Eqs. (16) and (17). From the table there appears to be a strong correlation between the value of k* and the vibrational temperature of the ground state of IF(X). Hence, an Arrhenius plot similar to Figures 15 and 16 was made and is shown in Figure 20. The solid line shown in the figure is the result of an analysis described below. The results of these experiments are presented in Table 3, listing the initial conditions for the reagent partial pressures, the vibrational temperatures of the two reagent species, NF(b) and IF(X) as well as that of the product excited molecule, IF(B).

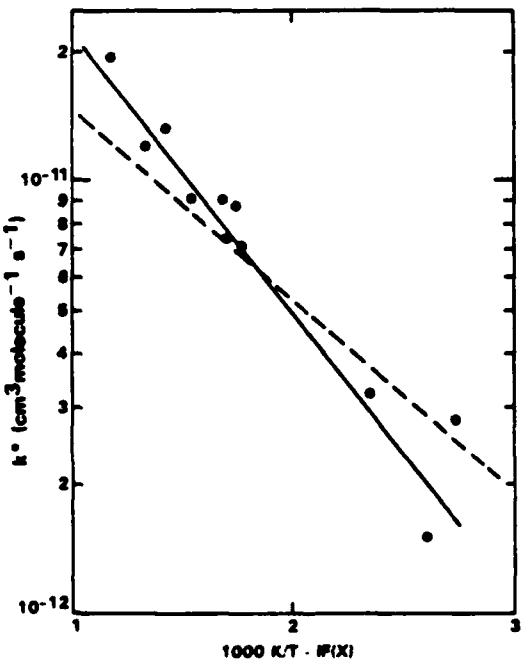

Fig. 20 Arrhenius plot of k* vs the reciprocal vibrational temperature of IF(X).

TABLE 3

E-E ENERGY TRANSFER RATE DATA

Pressures (mtorr)				Temperature (K)			k*
Total	F_2	HN_3	CF_3I	NF(b)	IF(X)	IF(B)	$10^{-11}cm^3/s$
100	116	17.9	10.5		907[a]	1229	7.08
747	70	16.8	11.7	672	597	790	0.90
843	74	6.0	11.3	863	749	652	1.20
1083	70	6.1	15.7	710	705	846	1.41
1198	79	6.7	15.8	758	566	755	0.87
980	62	9.5	18.8	815	428	891	0.32
969	61	8.2	19.8	443	367	961	0.28
1213	80	7.5	21.7	671	852	706	1.94
896	47	14.7	48.5	1124	652	1046	~ 0.9[b]
885	49	11.7	15.8	531	385	702	0.15
873	28	9.5	25	810	535	852	0.51
893	29	9.0	19.9	882	587	1146	0.73
1081	30	18.3	15.2	842	566	874	0.70

[a] The determination of this temperature is in doubt due to uncertainty of the laser power used to observe LIF signals.

[b] Uncertainty introduced due to $[F]<[CF_3I]$.

A multiple regression analysis was used to correlate the E-E energy transfer rate constant with the vibrational distributions of both NF(b) and IF(X). We assume that the correlation follows the population distribution of the two colliding species. The assumed relationship of the E-E energy transfer rate constant with the two vibrational temperatures, which are assumed to be independent, is expressed as follows:

$$k^* = k_o e^{-\alpha/kT_b} \quad e^{-\beta/kT_x} \tag{22}$$

where T_b and T_X are the vibrational temperatures describing the distributions of the NF(b) state and the IF(X) state, respectively. Taking the natural log of both sides of the equation linearizes the dependent variable with respect to the two independent variables. In the linear form, the dependent variable becomes ln k*, and the two independent variables are $1/T_b$ and $1/T_X$. The data transformed in this manner were subjected to linear least squares multiple regression analysis as described in Ref. 35, having the form

$$y = a_0 + a_1x_1 + a_2x_2 + \ldots \tag{23}$$

where $a_0 = \ln k_0$, $a_1 = -\alpha/k$, and $a_2 = -\beta/k$. The following values were obtained from the analysis:

$$\begin{aligned} a_0 &= -23.4 && (k_0 = 6.9 \times 10^{-11}\ \text{cm}^3\ \text{molecule}^{-1}\text{s}^{-1}) \\ a_1 &= -378 \pm 250\ \text{K} && (\alpha = -126 \pm 85\ \text{cm}^{-1}) \\ a_2 &= 1703 \pm 300\ \text{K} && (\beta = 1135 \pm 200\ \text{cm}^{-1}) \end{aligned} \tag{24}$$

The negative value of α suggests that, as the energy stored in the vibrational manifold of NF(b) is increased, the E-E energy transfer rate constant is reduced. We have, therefore, plotted a reduced form of the rate constant by dividing the rate constant by the IF(X) Boltzmann term $[\exp(-1703/T_X)]$ against $1/T_b$. This plot is shown in Figure 21. Note that, although the linear least squares analysis yields a negative value for α, the scatter in the data shown in Figure 20 suggests that the E-E rate constant is not correlated well with

Ref. 35 P. Bevington, Data Reduction and Error Analysis for Physical Sciences (McGraw-Hill Book Co., Inc., 1969).

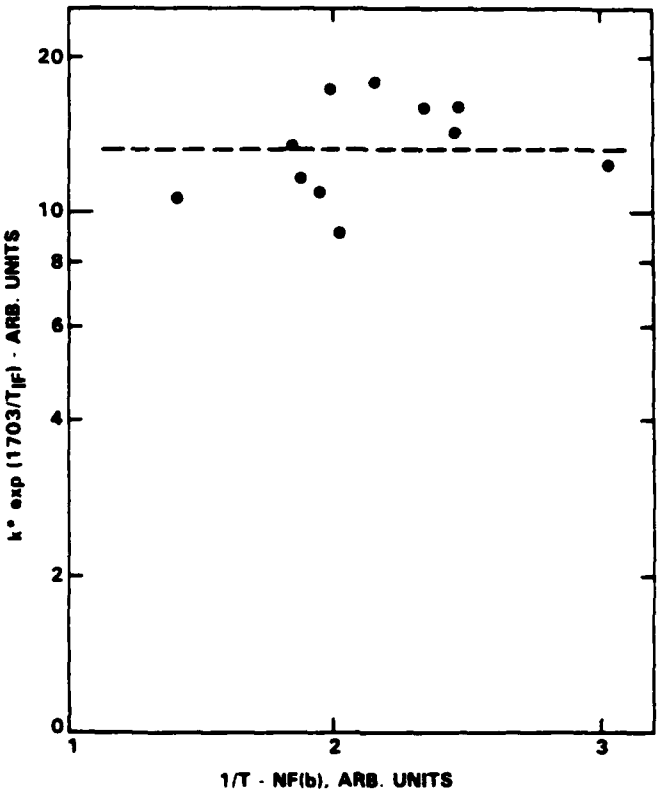

Fig. 21 Arrhenius plot of k* adjusted for the dependence of the vibrational temperature of IF(X) vs the reciprocal vibrational temperature in NF(b).

the vibrational temperature of NF(b), i.e., the E-E energy transfer rate constant is independent of the vibrational temperature in NF(b).

In summary, the E-E energy transfer rate constant is strongly dependent on the vibrational temperature of IF(X), see Figure 20 and independent of the vibrational temperature of NF(b), see Figure 21. In addition, the vibrational temperature of the product IF(B) is always greater than the vibrational temperature in the IF(X) state. The total rate constant by which NF(b) transfers its energy into IF(X) at 800 K is 1.5×10^{-11} cm^3/molecule/s.

The random errors in determining the E-E energy transfer rate constant stem primarily from the measurement of the concentration of RI (hence, IF(X)) in the flow. Two possible systematic errors are the NF(b) radiative rate A_b used in Eq. (16) and the degree of mixing in the flow tube.

V. EFFICIENCY OF THE NF/IF ENERGY TRANSFER PROCESS

In the previous section, the E-E rate constant between NF(b) and IF(X) was determined as a function of the vibrational energy distribution in NF(b) and IF(X). Although the rate is moderately fast (30-300 gas kinetic collisions), the total rate by which IF(X) quenches the electronic energy of NF(b) was not determined. This section addresses the total quenching rate issue. As in the previous section, two methods were employed to determine the total NF(b) quenching rate constant by IF(X). These methods include both steady-state and time-resolved techniques.

1. STEADY-STATE METHOD

The b state of NF is produced in the pooling reaction of NF(a) with vibrationally excited HF, requiring two quanta of vibrational energy in HF. The total pooling reaction rate is considered to be nearly gas kinetic, and the equilibrium constant for the pooling process is on the order of unity. Under these fast kinetic conditions, quenching of any energy-rich species (NF(b), NF(a), or HF(v)) in the equilibrium will be reflected by a decrease of concentration of the other species. By monitoring the decay of NF(b) in the flow tube apparatus, we are observing the decay of all the species in the equilibrium pooling process. To determine the quenching of the NF(b) by any selected molecule, the observed decay must be corrected by the decay of NF(a) and HF(v) by the same molecule.

The quenching of NF(a) by the addition of CF_3I was determined in a separate flow tube experiment. In this experiment HN_3 was added to the F atom stream through the annular injector. Trifluoromethyliodide was added through the central injector 8 cm downstream of the annular injector. The distance between the two injectors was sufficient for the F atoms to completely react with HN_3 and for the NF(b) and HF(v) to collisionally decay. Under these conditions, the CF_3I was added to a flow of F atoms, F_2, NF(a), and vibrationally cold HF. The decay of NF(a) was then monitored as a function of distance

down the flow tube for each initial concentration of CF_3I added to the flow. The decays were exponential, as shown in Figure 22. A plot of the decay rate vs the added CF_3I partial pressure is presented in Figure 23. As can be observed in the Stern-Volmer plot, the data do not appear to follow a linear relationship; however, a best fit was applied to the data for use in determining the efficiency of the E-E transfer process.

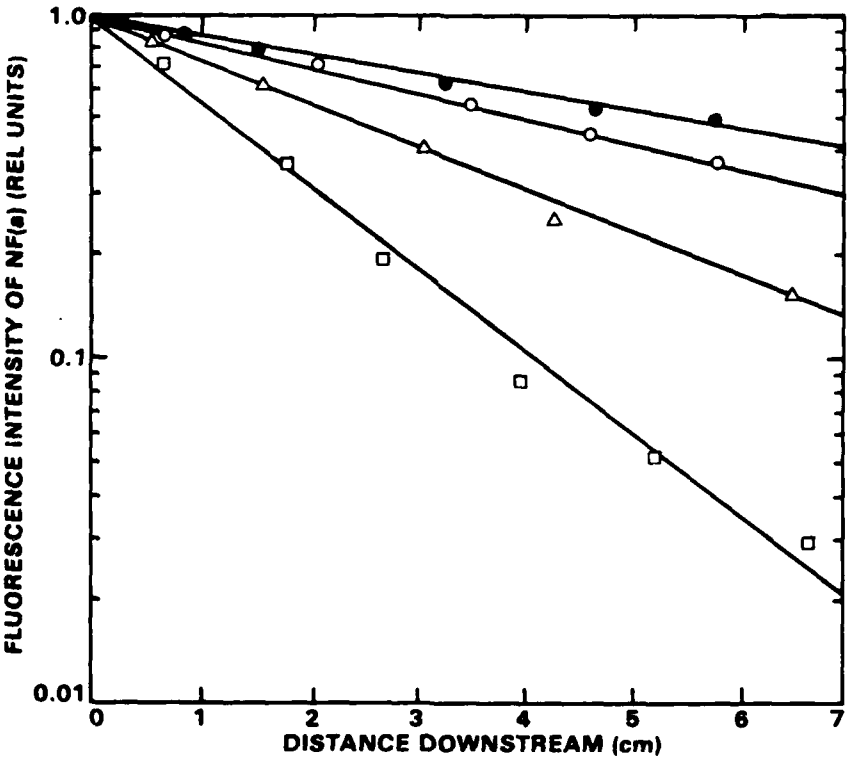

Fig. 22 Decay of the NF(a) fluorescence as a function of distance downstream of the CF_3I injection point.

The efficiency of transferring energy from NF(b) to IF(X) was determined by taking the ratio of the E-E energy transfer rate constant to the total NF(b) quenching rate constant. The E-E energy transfer rate constant was determined using Eq. (24). The total quenching of NF(b) by the addition of CF_3I to the flow was measured and corrected for the quenching of

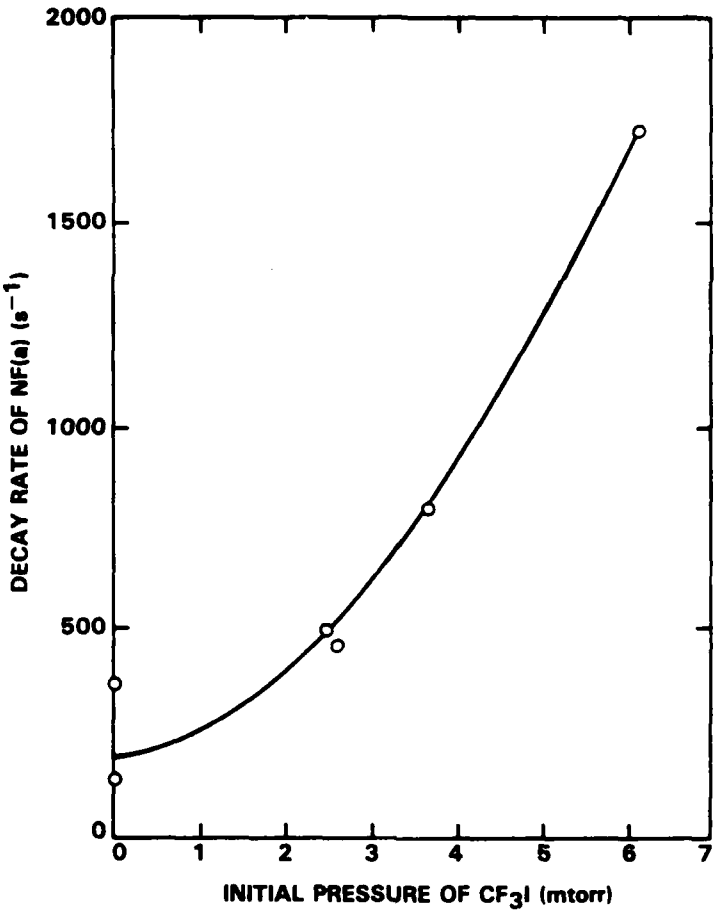

Fig. 23 Rate of NF(a) quenching by added CF_3I to the flow.

NF(a). The decay of NF(b) along the flow tube was exponential with and without the addition of CF_3I. A typical decay plot of the intensity of the NF b-X emission vs the distance along the flow tube is presented in Figure 24. The difference in these decay rates as a function of the partial pressure of CF_3I is presented in Figure 25. In some experiments, the initial flow rates of the CF_3I were recorded as the actual flow rates, but we discovered that when the flow rates were adjusted, the time to reach steady-state values was longer than anticipated. Hence, two of the data points, as indicated in the figure, lie far off the best fit of the data. For these two data points, we have used the decay difference to establish the partial pressure of CF_3I. The total quenching rate for NF(b) by the presence of CF_3I was adjusted to reflect the quenching of NF(a) using the following formula:

$$k_T = \left(\frac{\Delta \text{ Decay rate}}{P_{CF_3I}} - 341 \right) 1000 \ (\text{torr}^{-1}\text{s}^{-1}) \qquad (24)$$

where P_{CF_3I} is the partial pressure (mtorr) of CF_3I. The value 341 is the total rate constant for quenching NF(a) by CF_3I, as determined from the fit of the data in Figure 23. The factor 1000 converts from mtorr units to torr units. For each of the data points shown in Figure 25, the E-E energy transfer rate constant was determined using the same procedure described in the previous section. Spectra were taken from 450-650 nm and selected integrated bands of the IF B-X spectra were corrected for the cube of the wavelength, for their respective Franck-Condon factors, and for the instrument response to determine individual rate constants for populating each v' level of IF(B). The individual rate constants were then summed to obtain the total E-E energy transfer rate constant, k*. The efficiency, therefore, is reported as k^*/k_T. Presented in Table 4 is a summary of the data used to determine this efficiency. For these experiments, the HN_3 and molecular fluorine flows were held constant while adjusting the flow of the CF_3I/Ar mixture.

TABLE 4

DATA FOR DETERMINING E-E ENERGY TRANSFER EFFICIENCY

Partial Pressure	ΔDecay (s^{-1})	k* ($10^5 s^{-1} torr^{-1}$)	k_T ($10^5 s^{-1} torr^{-1}$)	Efficiency
1.91	1832	2.0	6.2	0.32
1.08	1082	2.1	6.6	0.31
0.54[a]	526	2.6	6.3	0.41
0.45	481	0.53	7.3	0.07[b]
1.09	1232	2.5	7.9	0.31
1.18	1393	8.4	8.4	1.00

[a] Partial pressure determined by the decay rate of NF(b).
[b] This value is highly inaccurate due to inaccuracy of determining the decay rate of NF(b) and of NF(a).

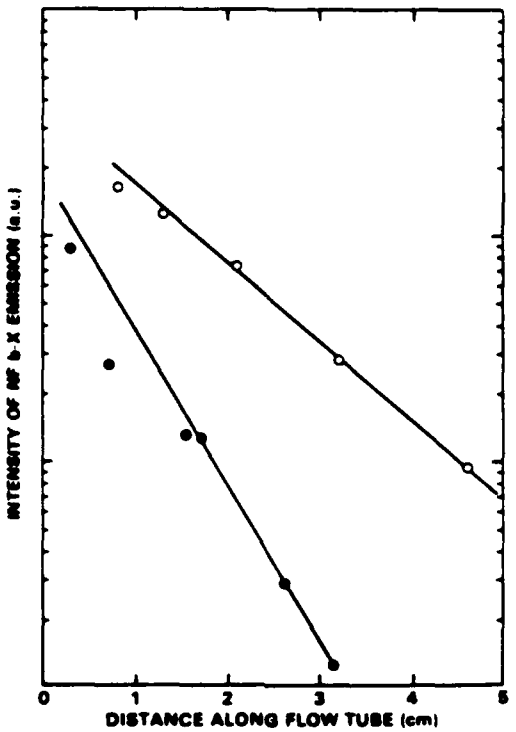

Fig. 24 Decay of NF(b) emissions as a function of distance down the flow tube.

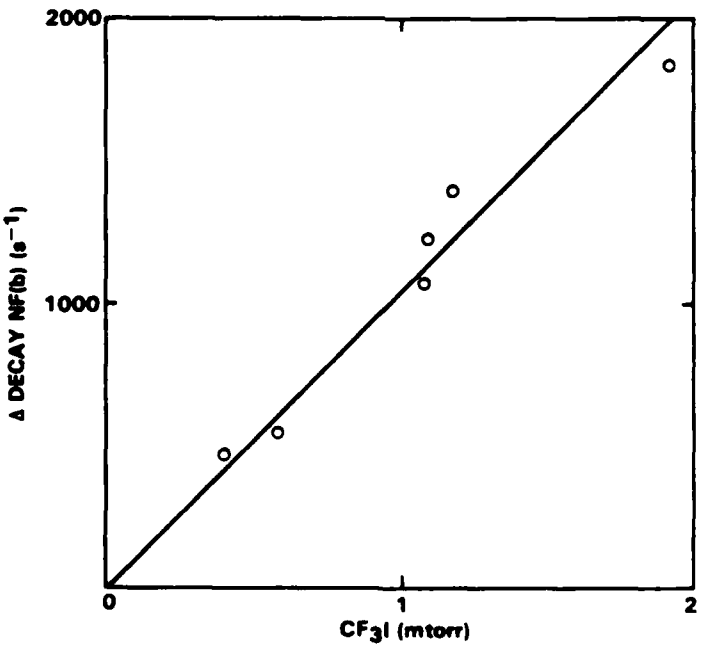

Fig. 25 Difference in the decay rate of NF(b) due to the pressure of added CF_3I.

For the data presented in Table 4, the energy transfer efficiency is typically greater than 30%. In this determination, we have not considered quenching of vibrationally excited HF by the addition of CF_3I, nor have we considered quenching of NF(b) by reaction products other than IF. Hence, the efficiency value represents lower bounds. Errors were encountered when the difference in the decay of NF(b), with and without the addition of CF_3I, was small. This problem was further complicated after subtracting the effects due to quenching of NF(a) by CF_3I. Hence, the reported values for lower CF_3I concentration would be expected to be highly inaccurate. To insure a margin of error associated with determining the lower bounds to the energy transfer efficiency, we report an E-E energy transfer efficiency of greater than 20%.

2. PULSED METHOD

We have investigated the efficiency of the E-E energy transfer process using pulsed techniques. In this technique, transient concentrations of I* were generated using the I* photolysis laser, as was done in the verification experiments. Unfortunately, the laser power had significantly declined due to leaks associated with the CF_3I gas handling system in the laser and due to the failure of the storage capacitor. Hence, we have reviewed the data obtained in the verification experiments for possible extraction of the total quenching rate of NF(b) by IF.

Production of NF(b) by the I* + NF(a) pooling reaction present problems similar to the HF(v) + NF(a) method of generating NF(b). The I* + NF(a) pooling reaction is also fast with an equilibrium constant near unity. Hence, the observed decay of the NF b-X fluorescence represents quenching of energy contained in the equilibrium reaction. The quenching of NF(a) and I* by IF and I (due to the addition of I_2 to the fluorine atom flow), therefore, must be determined and the effects deconvoluted from the

observed NF(b) decay. Quenching of I* by IF has been observed and a preliminary quenching rate constant of 6×10^{-12} cm^3/molecule/s has been obtained.† The quenching of NF(a) by the addition of I_2 was determined in a manner similar to that which was done for CF_3I. Hence, plots of the decay of the NF a-X emission intensity along the flow tube were constructed and the decay rates were obtained from these plots for a number of initial I_2 partial pressures. A Stern-Volmer plot of the NF(a) decay rates vs the I_2 partial pressure is presented in Figure 26. The slope of the best fit of the data indicates a quenching rate constant of 2×10^6 $torr^{-1}s^{-1}$. This rate constant is much larger than the one obtained in the CF_3I quenching experiments (Figure 23). The results suggest that, as long as the initial IF concentrations are similar in both experiments, the increased quenching must be due to the presence of iodine atoms. In this regard we note that in the I* + NF(a) energy pooling studies of J. Herbelin (Ref. 2), in which the iodine atom concentrations were much larger than they are for this study, a rate constant of $< 8 \times 10^{-13}$ cm^3/molecules/s was implied for the quenching of NF(a) by iodine atoms. This value is over two orders of magnitude less than the one found here for the addition of I_2. Reactions of NF(a) with iodine atoms would be expected to be slow due to spin-selection rules which are expected to apply for NF(a) (Refs. 27 and 36). Deactivation of NF(a) is also unlikely to be efficient, in that over 3800 cm^{-1} of energy must be dissipated into translation or channeled into vibrational energy of NF(X), resulting in populating the v"=3 level which represents a significant change to the nuclear motion of NF.

The quenching studies for NF(a) are not species specific but rather added reagent specific. The studies of the phenomenological quenching of NF(a) by the added gases (CF_3I or I_2) are sufficient for correcting the

---

†Work done at Rockwell International Science Center IR&D program (1983).
Ref. 36 J.M. Herbelin, Chem. Phys. Lett. 42, 367 (1976).

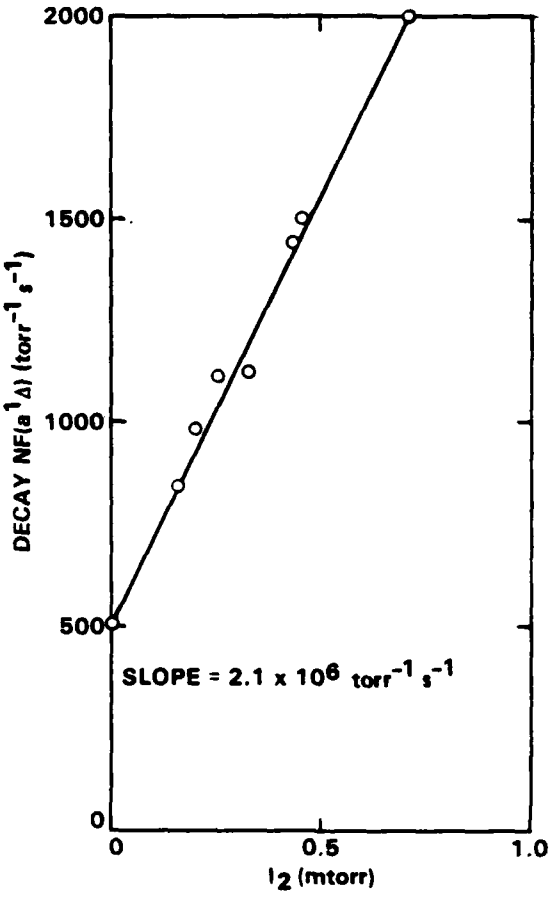

Fig. 26 Rate of NF(a) quenching by I_2 added to the flow.

observed decays of NF(b) produced by the pooling reactions, since the conditions of the flow tube were similar for both sets of experiments. The quenching studies of NF(a), and of NF(b) for that matter, were done for one set of operating conditions in the flow tube. A much more intensive study would be required to eliminate possible experimental artifacts which influence the observed decays in NF(a) and NF(b) and to identify specific quenchers.

The fast NF(a) quenching by adding I_2, when applied to the data obtained in the verification experiments, results in very low or negative values for the quenching of NF(b) by I_2 (or IF). Given these results, quoting efficiencies greater than unity or negative values is of no use. The major problem with the available data from the verification study is that the initial concentrations of HN_3 or DN_3 were not constant. Small variations

in the initial concentrations strongly affect the overall quenching of NF(a), I*, and NF(b). Hence, it is difficult to compensate adequately from one set of experimental conditions to another. The goal was to obtain NF b-X temporal profiles in which all variables were held constant except for the I_2 concentration, a goal not realized due to the failure of the I* photolysis laser.

VI. CONCLUSIONS AND RECOMMENDATIONS

In Section IV the E-E energy transfer rate constant was determined to be strongly dependent on the vibrational distribution in the ground state of IF and independent of the vibrational distribution of NF(b). In addition, the value of the vibrational temperature in the product state IF(B) is greater than that of the vibrational temperature in the reagent IF(X). These observations can be explained by an empirical model which favors vertical transitions of both NF and IF in the energy transfer process. John Herbelin[†] suggested that the individual rate constants for populating a given v' level in the B state of IF can be related to the Franck-Condon factors associated with the transfer of energy from NF(b) and with the reception of this energy by IF. This concept takes the following form:

$$k_{v'} = k_o \sum_{v',v''}^{NF} q_{NF}(v', v'') \sum_{v''}^{IF} q_{IF}(v', v'') \, e^{-\Delta E/E_o} \qquad (25)$$

where k_o is some effective collision rate constant, the q's are the Franck-Condon factors for the transitions in NF and IF; ΔE is the energy defect for each state-to-state reaction,

$$NF(b,v') + IF(X, v'') \rightarrow NF(X,v'') + IF(B,v') + \Delta E \qquad (26)$$

and E_o is a parameter which reflects the time scale (h/E_o) over which the electronic energy transfer takes place. The implication of Eq. (25) is that the transfer of electronic energy occurs in a time period short compared to the period of a vibration for the reagent molecules. For Eq. (25) we have selected an average vibrational energy, i.e.,

[†]Private communication, J.M. Herbelin (1984).

$$E_0 = 1/2[(\omega_e(NF(b)) + \omega_e(IF(X))] \quad (27)$$

This empirical approach satisfies most of the observations to date on the E-E energy transfer process. The insensitivity of the rate constant to the vibrational distribution in NF is explained by the Franck-Condon factors for the NF b-X transition. Since the potential curves for the b and X states are not displaced from each other, the Franck-Condon factors favor the $\Delta v = 0$ progression. The energy to be transferred from NF(b) to IF(X), therefore, is nearly constant, no matter which vibrational level of the b state is available, thus leading to the observed independence of the vibrational temperature of NF(b). The potential curves of the B and X states of IF, however, are highly displaced. Since the energy to be transferred from NF(b) is constrained to a fixed value, only a few channels, due to the near-resonance condition imposed by the exponential term in Eq. (25), are available to receive this energy. The T_0 values for NF(b) and IF(B) are nearly equal ($\Delta E = 50\ cm^{-1}$) and, therefore, in transferring energy from NF(b) to IF(X), the most favored channels for excitation in IF by the exponential factor are those associated with the $\Delta v = 0$ transitions in IF. The Franck-Condon factors for the 0-0, 1-1, 2-2, and 3-3 transitions in IF corresponding to the near resonant channels are 0.00482, 0.08927, 0.09939, 0.02468, respectively. The sensitivity of the vibrational temperature can be readily understood in terms of these factors. At low vibrational temperatures, most of the population of the v" levels in IF(B) ($\omega e = 610\ cm^{-1}$) reside in v"=0. Application of Eq. (25), therefore, results in small probabilities for the E-E energy transfer. As the vibrational temperature is increased, populations in v"=1 and 2 increase, and with the application of Eq. (25) the probability of the E-E energy transfer process is enhanced.

Eq. (25) was used to calculate the total E-E energy transfer rate constant ($k^* = \Sigma\ k_{v'}$) as a function of the vibrational temperature in IF. For this calculation we assumed,

$$q_{NF}(v',v'') = \delta\ (v',v'') \qquad (28)$$

which is nearly correct. Use of the actual Franck-Condon factors as reported by Mohammed, et al (Ref. 31), does not substantially change the results. The value of k_0 was selected to be 1×10^{-10}, a rate constant which corresponds to about three gas kinetic collisions. The calculated rate constant was plotted against the reciprocal vibrational temperature of the IF(X) state and compared to the observed values. This plot is shown as the hashed line in Figure 20. Only the k_0 term was selected for matching the observed values to the calculated ones. The activation energy, expressed as the slope of the best fit to the data in Figure 20 (the solid line), is explained well by this vertical transition procedure. The calculated activation energy (= 1462 cm^{-1}) is within 1σ of the error bounds of the observed activation energy.

In addition to the total E-E rate constant, the nascent vibrational distribution can also be calculated and compared to the observed vibrational distributions. For convenience we have calculated the vibrational temperature of the nascent distributions determined from the application of Eq. (25) using the following definition:

$$T = \Sigma\ E_{v'}\ f_{v'}/k \qquad (29)$$

where $f_{v'}$ represents the fraction of the B state production entering the v' level and k is the Boltzmann constant. We have generated a plot of the above calculated temperature as a function of the initial vibrational temperature of IF(X) (Figure 27). In our experiments, however, some vibrational relaxation can occur before the IF(B) emits. The observed vibrational distributions, therefore, are not the nascent ones from the E-E energy transfer process. The data shown in Figure 27 would not be expected to match the calculated values

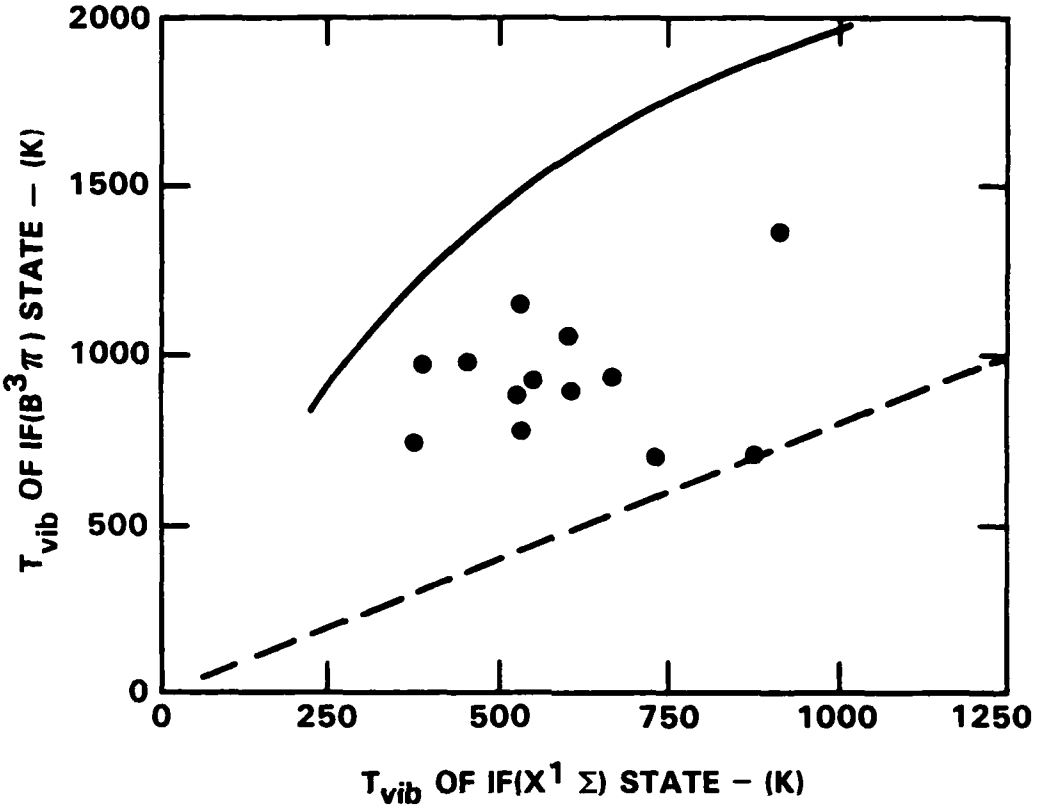

Fig. 27 Plot of the IF(B) vibrational temperature vs the IF(X) vibrational temperature.

which do not take into account loss of energy from the vibrational mainfold via V-R,T processes. The vibrational quenching rate constants for deactivation of the vibrational states of IF(B) have been determined by Davis, et al.[†] The rate constant for deactivation (T = 300 K) of v'=3 by argon is $3 \times 10^{-12} cm^3$/molecule/s. This rate constant implies that approximately 100 collisions are required to deactivate v'=3 to 1/e of its original value. At 1 torr, there are approximately 50 gas kinetic collisions during the radiative lifetime of the B state. Hence, the observed vibrational distributions for the lower pressure studies would be expected to more strongly reflect the nascent vibrational distributions. As can be observed in Figure 27, the data

[†]S.J. Davis, AFWL, private communication, 1984.

fall in a region between the calculated vibrational distributions and the thermal bath temperature, as shown by the dashed line. This result is consistent with the preceding analysis which predicts the temperature dependence of the total rate constant quite accurately. Experiments must be conducted at much lower total pressures before the true nascent distributions can be observed.

Although the empirical expression does much to describe the salient features observed for the E-E energy transfer rate constant, the mechanism for the transfer is not identified. The transfer of electronic energy involves potential energy curve crossings. These crossings can take place in either the short-range regions of the potential curves, usually at the turning points, or the long-range portions of the curves. In long-range force theories, the transfer probability is increased as the time for passage through the crossing zone is increased. This leads to an overall increase in the rate constant for lower temperatures. On the other hand, short-range force theories favor increased transfer probabilities as the energy of the colliding partners is increased. This phenomenon is a consequence of the necessity of tunneling from one curve to another at the turning point. In Figure 20, the observed rate constants are more sensitive to the vibrational temperature in IF(X) than are the calculated rate constants. Apart from the k_o term in Eq. (25), the expression is independent of velocity of the colliding partners. A mechanism based on a short-range theory appears to be the appropriate one. This conclusion is not a strong one, because the match between the observed and calculated rate constants is so close. Another argument in favor of a short-range theory centers on the time scale for the interaction. In long-range force theories, the accelerating forces are not particularly strong, and the time to traverse the crossing zone at thermal temperatures would be on the order of several vibrational periods of the colliding partners. Hence, the selectivity of the Franck-Condon factors, which appear to play a strong role in the rate constant, would be eliminated,

since during the transfer of electronic energy the nuclear motions could adjust to statistical distributions. The time to pass through the crossing zone at the turning points, however, can be much shorter than a vibrational period.

The rate constant for the transfer of electronic energy from NF(b) to IF(X) is sufficiently fast to consider the use of this E-E energy transfer process to collisionally pump IF to lasing. As has been demonstrated by Davis and his co-workers at the AFWL,* optical pumping of IF to lasing by a CW pump laser demonstrates that a total inversion of the B state is not necessary. The success of developing a chemical laser based on this energy transfer process centers on the means by which sufficient quantities of NF(b) can be generated. Large quantities of NF(b) have been generated at the Aerospace Corporation by optically pumping atomic iodine in the presence of large quantities of NF(a) (Ref. 2). Since all methods of generating NF(b) are based on the utility of NF(a), the chemistry of generating NF(a) must be compatible with the presence of IF.

Based upon this discussion, we recommend that a concept be chosen based upon its feasibility for developing a chemical laser. Once the system has been selected, specific elementary reaction rate constants should be determined which would impact the efficiency of the device. In addition, scaling studies should be started to discover possible second-order reactions which would limit the ultimate size of the chemical laser. Finally, the scaling studies should be pursued to sufficient levels to establish a valid gain demonstration.

This discussion is based on a possible laser demonstration given our current knowledge about NF(b) generation. Basic research studies should be initiated to find chemical means of generating NF(b) directly in a chemical reaction or energy efficient process. Success in this effort would circumvent

*S.J. Davis, et al, AFWL, presented at the Short Wavelength Chemical Laser Workshop, Charleston, S.C., November 15, 1984.

the need for producing NF(a) and for employing an energy pooling scheme to generate NF(b). Also, studies to generate other metastable species which could transfer their energy to possible lasant molecules should be pursued. For example, NH(a) and NH(b) would make excellent energy storage species. Finally, continued studies in E-E energy transfer processes to identify new systems and to uncover the underlying mechanism would be of great assistance in developing a short-wavelength chemical laser.

REFERENCES

1. J.M. Herbelin, D.J. Spencer, and M.A. Kwok, J. Appl. Phys. 48, 3050 (1977).

2. J.M. Herbelin, M.A. Kwok, and D.J. Spencer, J. Appl. Phys. 49, 3750 (1978).

3. P.L. Byer, R.L. Herbst, H. Kildal, and M.D. Spencer, J. Appl. Phys. 49, 3750 (1978).

4. S.R. Leone and K.G. Kosnik, Appl. Phys. Lett. 30, 346 (1977).

5. F.J. Wodarczyk and H.R. Schlossberg, J. Chem. Phys. 67, 4476 (1977).

6. W.P. West and H.P. Broida, Chem. Phys. Lett. 56, 283 (1978).

7. J.B. Koffend and R.W. Field, J. Appl. Phys. 48, 4468 (1977).

8. S.J. Davis and L. Hanko, Appl. Phys. Lett. 77, 692 (1980).

9. S.J. Davis, L. Hanko, and R.F. Shea, J. Chem. Phys. 78, 172 (1983).

10. A.T. Pritt Jr., D. Patel, and D.J. Benard, Chem. Phys. Lett. 97, 471 (1983).

11. R.D. Coombe, D. Patel, A.T. Pritt Jr., and F.J. Wodarczyk, Chemical Production of Excited NF, AFWL-TR-81-211, Air Force Weapons Laboratory, Kirtland AFB, NM, July 1982.

12. J.R. McDonald, J.W. Rabalais, and S.P. McGlynn, J. Chem. Phys. 52, 1332 (1970).

13. L. Gillespie and L. Fraser, J. Amer. Chem. Soc. 58, 2260 (1936).

14. J.G. Calvert and J.N. Pitts, Photochemistry (John Wiley and Sons, Inc., New York, 1966) 184.

15. A. Fontijn, C.B. Meyer, and H.I. Schiff, J. Chem. Phys. 40, 64 (1964).

16. T. Trickl and J. Wanner, J. Mol. Septrosc. 104, 174 (1984).

17. M.A.A. Clyne and I.S. McDermid, J. Chem. Soc. (Faraday II) 72, 2252 (1976).

18. R.D. Coombe and A.T. Pritt Jr., Chem. Phys. Lett. 58, 606 (1978).

19. A.T. Pritt, Jr., D. Patel, and R.D. Coombe, Int. J. Chem. Kinetics 16, 977 (1984).

20. M.A. Kwok, J.M. Herbelin, and N. Cohen, Electronic Transition Lasers (MIT Press, Cambridge, MA, L.E. Wilson, et al., eds., 1976) 8.

21. J.T. Yardley, Introduction to Molecular Energy Transfer (Academic Press, Inc., New York, 1980).

22. M.A. Kwok and J.M. Herbelin, Electronic Transition Laser II (MIT Press, Cambridge, MA, L.E. Wilson, et al, ed., 1977) 100.

23. S.R. Leone, Adv. Chem. Phys. 50, 255 (1982).

24. J.J. Sloan, D.G. Watson, and J.S. Wright, J Chem. Phys. 43, 1 (1979).

25. A.T. Pritt Jr., and D. Patel, J. Chem. Phys. 81, 1337 (1984).

26. L.G. Piper, R.H. Krech, and R.L. Taylor, J. Chem. Phys. 71, 2099 (1979).

27. C.T. Cheah and M.A.A. Clyne, J. Chem. Soc. (Faraday II) 76, 1543 (1980).

28. J.M. Herbelin and M.A. Kwok, Electronic Angular Momentum Transfer in the $I^2P_{1/2}$) + NF(a'Δ) System, SAMSO-TR-76-62, The Aerospace Corporation, El Segundo, CA (1976).

29. R.J. Malins and D.W. Setser, J. Phys. Chem. 85, 1342 (1981).

30. P.H. Tennyson, A. Fontijn, and M.A.A. Clyne, Chem. Phys. 62, 171 (1981).

31. K.A. Mohamed, B.N. Khanna, and K.M. Lal, Ind. J. Pure Appl. Phys. 12, 243 (1974).

32. P.S. Ganguli and M. Kaufman, Chem. Phys. Lett. 25, 221 (1974).

33. A.T. Pritt Jr., Excited State Chemistry of Halogen Azides, AFOSR Report No., AF Office of Scientific Research, Bolling AFB, DC (1982).

34. A.T. Pritt, Jr. and R.D. Coombe, Int. J. Chem. Kinetics 12, 743 (1980).

35. P. Bevington, Data Reduction and Error Analysis for Physical Sciences (McGraw-Hill Book Co., Inc., 1969).

36. J.M. Herbelin, Chem. Phys. Lett. 42, 367 (1976).

END

DTIC

8-86